DEVELOPMENTAL BIOLOGY

Identification and characterization of BEND2 as a key regulator of meiosis during mouse spermatogenesis

Longfei Ma[1,2,3,4]†, Dan Xie[1,2,3,4]†, Mengcheng Luo[5], Xiwen Lin[1,2,3], Hengyu Nie[1,2,3,4], Jian Chen[1,2,3], Chenxu Gao[1,2,3,4], Shuguang Duo[6]*, Chunsheng Han[1,2,3,4,6]*

The chromatin state, which undergoes global changes during spermatogenesis, is critical to meiotic initiation and progression. However, the key regulators involved and the underlying molecular mechanisms remain to be uncovered. Here, we report that mouse BEND2 is specifically expressed in spermatogenic cells around meiotic initiation and that it plays an essential role in meiotic progression. *Bend2* gene knockout in male mice arrested meiosis at the transition from zygonema to pachynema, disrupted synapsis and DNA double-strand break repair, and induced nonhomologous chromosomal pairing. BEND2 interacted with chromatin-associated proteins that are components of certain transcription-repressor complexes. BEND2-binding sites were identified in diverse chromatin states and enriched in simple sequence repeats. BEND2 inhibited the expression of genes involved in meiotic initiation and regulated chromatin accessibility and the modification of H3K4me3. Therefore, our study identified BEND2 as a previously unknown key regulator of meiosis, gene expression, and chromatin state during mouse spermatogenesis.

INTRODUCTION

Meiosis is the fundamental component of gametogenesis and consists of multiple processes that occur either sequentially or concurrently (*1*). Meiosis is initiated when homologous chromosomes begin to pair and large-scale, programmed DNA double-strand breaks (DSBs) are generated (*2*). DSB repair and synapsis of homologous chromosomes are simultaneous and mutually dependent. Synapsis starts when the 3′ overhangs of DSBs invade homologous DNAs to form recombinant intermediates, and when the axial elements of the synaptonemal complex that consists of proteins such as SYCP3 and cohesin are bridged by SYCP1 and other central element components (*3*). Full synapsis is achieved when DSB repair intermediates are resolved into crossovers and the chromosomes become highly condensed around the complete synaptonemal complex.

These meiotic steps/processes are intricately coordinated by the complex interactions between chromatin and a large number of chromatin-binding proteins that include synaptonemal complex proteins, enzymes, chromatin modifiers/remodelers, and transcription factors. To give an example, PRDM9, which is the primary determinant of recombination hotspot locations, acts as both a histone-modifying enzyme and a pioneer transcription factor, and interacts either directly or indirectly with many proteins, including CXXC finger protein 1 (CXXC1), EWS RNA binding protein 1 (EWSR1), euchromatic histone lysine methyltransferase 2 (EHMT2), chromodomain Y like (CDYL), meiotic cohesin REC8, SYCP3, SYCP1, and lymphoid-specific helicase (LSH/HELLS) (*4*, *5*). An increasing number of meiotic regulators have been identified by genetic studies, using model organisms such as gene knockout (KO) mice; these meiotic regulators include chromatin remodelers/modifiers and transcription factors such as YY1 (*6*), SUV39H (*7*), PRDM9 (*8*), and SCML2 (*9*). Unfortunately, the spatiotemporal interactions between these regulators remain largely unknown. The concerted actions of these regulators usually result in chromatin states that are required for DNA activities such as DSB formation/repair, synapsis, and transcription (*10*). Specifically, correct chromatin states at particular genomic regions such as repetitive sequences and heterochromatin must be established to prevent erroneous recombination and/or transcription, which are detrimental to genome integrity (*6*, *7*).

In the present study, we report the identification of a previously unidentified meiotic regulator, BEND2, that belongs to a BEN domain–containing protein family that is poorly characterized. The BEN domain was first identified in diverse metazoan and viral proteins (usually with multiple copies) and was named after three experimentally characterized proteins—BANP, E5R, and NAC1—in which it is present (*11*). A total of nine human and mouse genes that encode BEND1 to BEND9 are found in each of the genomes of these two species according to the National Center for Biotechnology Information (NCBI) Gene database. Although studies on the BEN family members are limited, they reveal the following key points: (i) BEN proteins tend to interact with a variety of proteins, most likely in a context-dependent manner; (ii) most of the interacting proteins are components of transcription-repressive complexes involved in chromatin remodeling and/or modification; and (iii) BEN proteins can be sequence-specific DNA binding proteins (see Discussion for more details).

To our knowledge, there is no report regarding the functions of BEN proteins in germ cell development. In the present study, we showed that BEND2 is specifically expressed in spermatogenic cells shortly before and during prophase of meiosis I, and that BEND2 is essential for meiosis in male mice. We observed multiple meiotic defects in DSB repair and synapsis in male KO mice, such as complete spermatogenic arrest at zygonema. We also demonstrated that BEND2 interacts with multiple chromatin-binding proteins and that it regulates chromatin states and transcription by preferentially targeting simple sequence repeats. These results add to our understanding of the molecular mechanisms governing meiosis and cell-specific regulation of chromatin states in meiotic cells.

[1]State Key Laboratory of Stem Cell and Reproductive Biology, Institute of Zoology, Chinese Academy of Sciences, Beijing 100101, China. [2]Institute for Stem Cell and Regeneration, Chinese Academy of Sciences, Beijing 100101, China. [3]Beijing Institute for Stem Cell and Regenerative Medicine, Beijing 100101, China. [4]Savaid Medical School, University of Chinese Academy of Sciences, Beijing 100049, China. [5]Department of Tissue and Embryology, Hubei Provincial Key Laboratory of Developmentally Originated Disease, School of Basic Medical Sciences, Wuhan University, Wuhan, Hubei Province, China. [6]Institute of Zoology, Chinese Academy of Sciences, Beijing 100101, China.
*Corresponding author. Email: hancs@ioz.ac.cn (C.H.); duoshuguang@ioz.ac.cn (S.D.)
†These authors contributed equally to this work.

RESULTS

BEND2 is a previously unidentified protein that is specifically expressed in spermatogenic cells around the time of meiotic initiation

We were initially interested in identifying and analyzing the functions of long noncoding RNA (lncRNA) genes that are specifically expressed in spermatogenic cells. An X chromosome–linked lncRNA gene based on the NCBI gene annotation was one such candidate, as we found that its transcripts were specifically expressed in mouse testes based on our RNA sequencing (RNA-seq) analyses of mouse multiorgan transcriptomic data (*12*). While our study was ongoing, this gene (NCBI Gene ID: 108168453) was reannotated as encoding a protein (UniProt ID: A0A140LIQ5) belonging to the BEN family (*11*). As the orthologous protein in humans has been named BEND2, we suggest that this mouse protein also adopt the same name. Predicted homologous BEND2 proteins can be found in vertebrates from fish to humans, and the sequence identity between the mouse and human proteins is 34% (fig. S1, A and B). The predicted longest transcript of mouse *Bend2* contains 15 exons, of which exons 2 to 15 harbor a coding sequence for a protein of 728 amino acids (predicted molecular mass, 80 kDa) (Fig. 1A). In addition, several transcript variants were detected exclusively in mouse testes by reverse transcription polymerase chain reaction (RT-PCR) (Fig. 1B and fig. S1C).

We developed a rabbit polyclonal antibody to BEND2 (rpAb-B2-1) by using a synthetic polypeptide from amino acids 585 to 614 between the two BEN domains as the immunogen (fig. S1B). This antibody functioned appropriately in Western immunoblotting and immunohistochemical analyses (fig. S1, D to F). By using rpAb-B2-1 in Western blot assays, we detected two proteins that may be related to BEND2 in the testicular lysates: One was 140 kDa (p140), while the other was 80 kDa (p80) (fig. S1D). Intriguingly, p80, but not p140, could be consistently and specifically found in testes (fig. S1G). We subsequently developed a second rabbit polyclonal antibody to BEND2 (rpAb-B2-2) by using the polypeptide from amino acids 243 to 486 of mouse BEND2 as the immunogen. Intriguingly, rpAb-B2-2 recognized p140 but not p80, and it also detected a major nonspecific protein of approximately 100 kDa (fig. S1H). As nonspecific proteins were detected by these two rabbit polyclonal antibodies in Western blots (labeled with an asterisk in fig. S1, D and H), we decided to generate knock-in (KI) mice in which a 3xFLAG sequence was added to the N terminus of BEND2 (FLAG-BEND2) (Fig. 1C and fig. S1I). By using a mouse monoclonal antibody against FLAG (mmAb-FLAG), only p140 was detectable in the KI testes but not in the wild-type (WT) testes by Western blotting (fig. S1J). p140 was also specifically observed when FLAG-BEND2 complementary DNA (cDNA) was expressed in 293FT cells by both rpAb-B2-1 and mmAb-FLAG, suggesting that p140 protein was FLAG-BEND2 itself (fig. S1K).

We also excised separate gel pieces that contained the p140 and p80 bands, analyzed the proteins by mass spectrometry (MS), and found that BEND2 peptides were detected in the p140, but not in the p80 samples (fig. S1L and table S1). On the basis of these results, it is likely that p140 is the full-length BEND2, the mobility of which in SDS–polyacrylamide gel electrophoresis (PAGE) was altered due to either posttranslational modification(s) or unusual higher-order structures; p80 was either a shorter version of BEND2 lacking the N-terminal end or a nonspecific signal recognized only by rpAb-B2-1 despite its molecular mass matching the predicted size of BEND2. We next expressed the N- and C-terminal halves of BEND2 as FLAG-tagged proteins in 293FT cells (predicted molecular masses, 36 and 44 kDa, respectively) and found that the former migrated as a protein of 73 kDa, while the latter migrated at 55 kDa (fig. S1M). Sequence analyses showed that the N-terminal half of BEND2 was much more disordered and hydrophobic than the C-terminal half (fig. S1N). Therefore, it was appropriate that BEND2 displayed slower electrophoretic mobility due to its unusual sequence/structure at the N terminus.

By using FLAG-BEND2 KI mice and the mmAb-FLAG antibody, we confirmed that p140 was exclusively expressed in testes among all of the tissues we examined (Fig. 1D). Using immunostaining of FLAG-BEND2 in testicular sections that could be staged on the basis of hematoxylin staining, we found that the protein was highly expressed in preleptotene (plpSCs), leptotene (lepSCs), zygotene (zygSCs), and pachytene (pacSCs) spermatocytes from stages VII to III, and weakly in type B spermatogonia (SG-B) and pacSCs at stages V and VI (Fig. 1, E and F). Immunofluorescence imaging with higher magnification and a shorter exposure time revealed that the signals for FLAG-BEND2 in the nuclei of spermatocytes were punctate (Fig. 1G). These results indicated that BEND2 is an evolutionarily conserved protein and that it is specifically expressed in the nuclei of spermatogenic cells in a stage-specific manner, shortly before and after meiotic initiation.

KO of *Bend2* results in meiotic arrest at prophase I

We endeavored to assess the function of BEND2 by evaluating phenotypic changes in gene KO mice that were generated by using CRISPR-Cas9 technology. Several founder mice with different mutant alleles were acquired: one male with a mutant allele consisting of a 19–base pair (bp) deletion ($Bend2^{-19/Y}$), one female with an allele of a 4–kilo–base pair (kbp) deletion ($Bend2^{-4k/+}$) corresponding to a 104–amino acid deletion in the protein, and another female with an allele of a single-base insertion ($Bend2^{+1/+}$) (Fig. 2, A to C, and fig. S2, A and B). Both the $Bend2^{-4k/+}$ and the $Bend2^{+1/+}$ female founders were crossed with WT males to at least the F_2 generation for phenotypic evaluation (fig. S2C). BEND2 was undetectable in the male founder with a 19-bp deletion ($Bend2^{-19/Y}$) or mutant male offspring from the $Bend2^{+1/+}$ and $Bend2^{-4k/+}$ founder (Fig. 2C and fig. S2D). As genotyping of the −4k allele was more accessible, further phenotypic evaluation of the KO mice was conducted using $Bend2^{-4k/Y}$ mice at or after the F_2 generation.

The *Bend2* KO male mice were infertile and exhibited markedly smaller testes than their WT littermates (Fig. 2, D and E, and fig. S2, E and F), and fertility testing showed that *Bend2* mutant males were infertile (Fig. 2F and fig. S2G) and that they did not produce any haploid spermatids or spermatozoa (Fig. 2, G and H, and fig. S2H). A closer inspection of the hematoxylin and eosin (H&E)–stained testicular sections revealed that the KO testes contained spermatogonia, lepSCs, zygSCs, and Sertoli cells, but no other type of germ cell (Fig. 2G). We also frequently observed apoptotic cells with condensed nuclei, and their presence was confirmed by terminal deoxynucleotidyl transferase–mediated deoxyuridine triphosphate nick end labeling (TUNEL) assays (Fig. 2, G and I). Both the numbers of TUNEL-positive tubules and TUNEL-positive cells per tubule were significantly higher than the numbers in the WT testes (Fig. 2J). In contrast, the numbers of undifferentiated spermatogonial stem cells ($PLZF^+$) and Sertoli cells ($WT1^+$) were equivalent between KO and WT mice (Fig. 2, K to N). These results indicated that BEND2 plays a specific and essential role in meiosis in male mice.

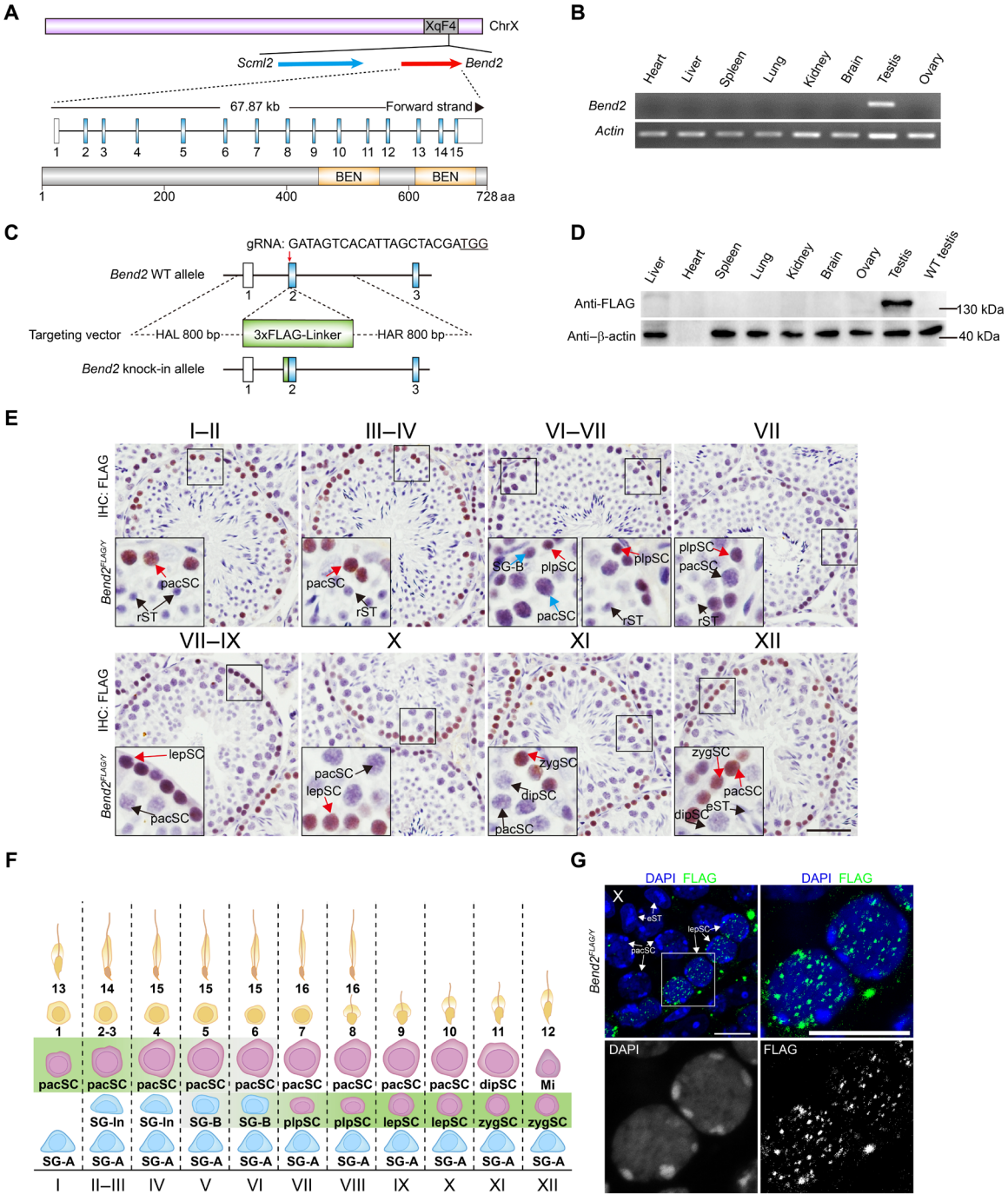

Fig. 1. BEND2 is specifically expressed around the time of meiotic initiation. (**A**) Schematic diagram of the primary structures of the *Bend2* gene and BEND2 protein. Top diagram shows the location of *Scml2* and *Bend2* genes in the X chromosome and the structure of the *Bend2* gene; blue and red arrows indicate *Scml2* and *Bend2* genes; blue and white rectangles indicate protein-coded exons and UTR regions, respectively. Bottom diagram represents the BEND2 protein, with orange boxes indicating the BEN domain. (**B**) RT-PCR detection of *Bend2* expression in multiple mouse organs. (**C**) Schematic representation of the locus of the 3xFLAG tag KI; the tag sequence was inserted immediately behind the first codon of BEND2. (**D**) Western blot analyses of BEND2 expression in multiple mouse organs using mmAb-FLAG. (**E**) Immunohistochemical (IHC) staining of FLAG-BEND2 in testicular sections of various seminiferous stages using mmAb-FLAG; red and blue arrows indicate BEND2 strongly and weakly expressing cells, respectively; black arrows indicate no BEND2 expression. SG-B, type B spermatogonia; plpSC, pre-leptotene spermatocytes; lepSC, leptotene spermatocytes; zygSC, zygotene spermatocytes; pacSC, pachytene spermatocytes; dipSC, diplotene spermatocytes; rST, round spermatids; eST, elongated spermatids. Scale bar, 20 μm. (**F**) Schematic summary of FLAG-BEND2 expression in male germ cell types and seminiferous stages. (**G**) Immunofluorescence staining of FLAG-BEND2 shown at higher magnification of BEND2 signals in lepSCs. Scale bars, 10 μm. aa, amino acids.

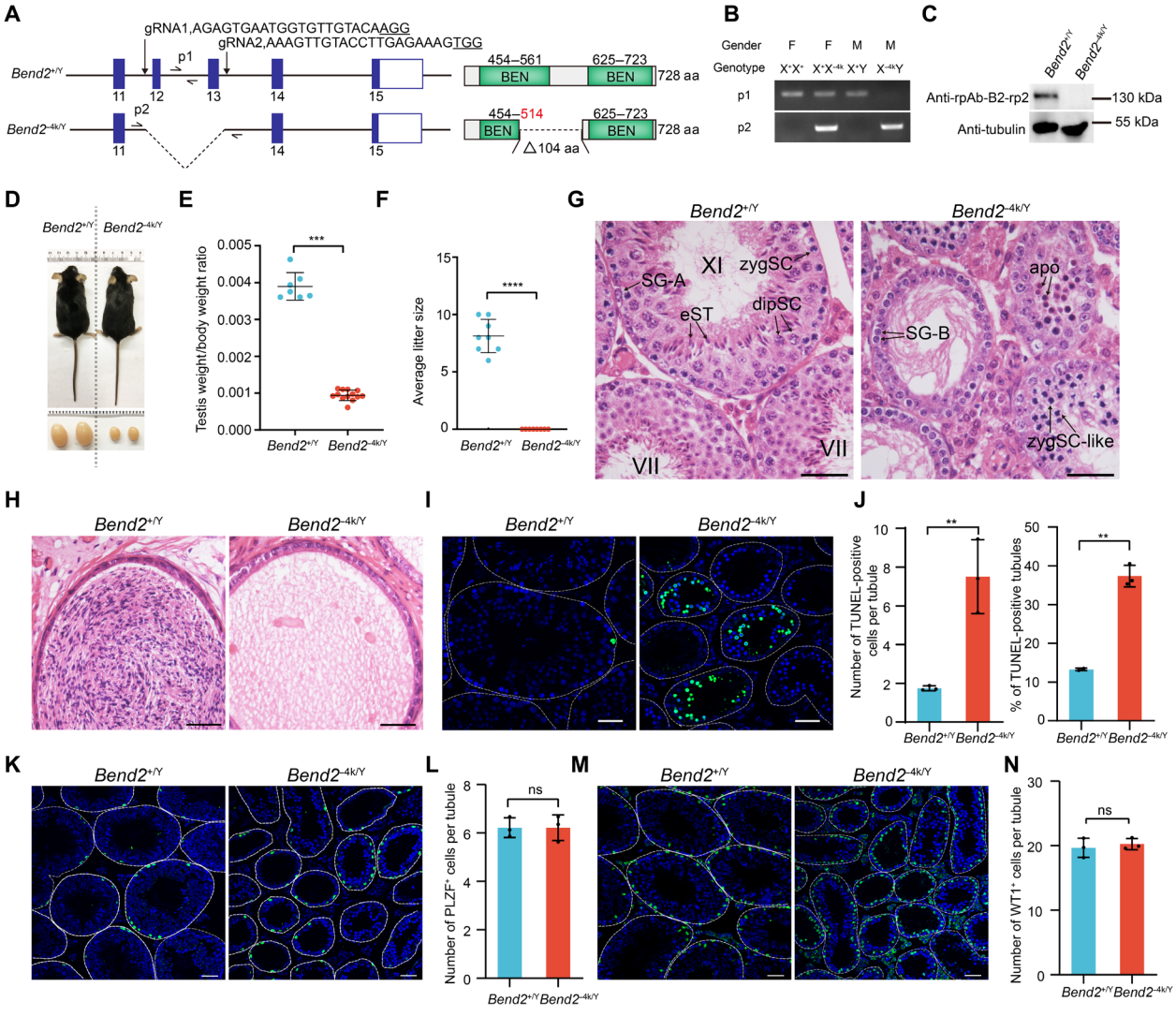

Fig. 2. BEND2 is required for mouse spermatogenesis and the maintenance of male fertility. (**A**) Schematic illustration of the deletion of two exons of the *Bend2* gene to generate *Bend2*$^{-4k/Y}$ mice; p1 and p2 indicate that two primers were used in mouse genetic identification. Right diagram shows BEND2 protein structure in WT and KO mice. (**B**) Identification of genotype with p1 (WT allele) and p2 (mutant allele) primer pairs. (**C**) Western blot confirmation of the elimination of BEND2 protein in *Bend2*$^{-4k/Y}$ mice using rpAb-B2-2. (**D**) Note the size reduction in 8-week-old *Bend2*$^{-4k/Y}$ testes. (**E**) Quantitative comparison of testis/body ratios between *Bend2*$^{+/Y}$ and *Bend2*$^{-4k/Y}$ mice (***$P < 0.001$, Student's *t* test). (**F**) Comparison of litter size in *Bend2*$^{+/Y}$ and *Bend2*$^{-4k/Y}$ mice (****$P < 0.0001$, Student's *t* test). (**G**) H&E staining of testicular sections in *Bend2*$^{+/Y}$ and *Bend2*$^{-4k/Y}$ mice. zygSC-like, zygotene-like spermatocytes; apo, apoptotic cells. Scale bars, 20 μm. (**H**) H&E staining of epididymal sections of *Bend2*$^{+/Y}$ and *Bend2*$^{-4k/Y}$ mice. Scale bars, 20 μm. (**I**) TUNEL staining of testicular sections in *Bend2*$^{+/Y}$ and *Bend2*$^{-4k/Y}$ mice; green signals indicate apoptotic cells. Scale bars, 50 μm. (**J**) Quantitative comparison of TUNEL staining shows that both TUNEL-positive cells and tubules were increased in *Bend2*$^{-4k/Y}$ mice. (**K** and **L**) Immunofluorescence staining indicates that the number of PLZF-positive cells (green) was the same between *Bend2*$^{+/Y}$ and *Bend2*$^{-4k/Y}$ mice. Scale bars, 20 μm. (**M** and **N**) Quantitative comparison of WT1 immunofluorescence staining of testicular sections in *Bend2*$^{+/Y}$ and *Bend2*$^{-4k/Y}$ mice. Scale bars, 20 μm. ns, not significant.

BEND2 occupies a role in DSB repair and synapsis

We next examined the molecular defects in the KO spermatocytes by immunostaining marker proteins involved in meiosis. The substages of meiotic prophase I that include leptonema, zygonema, pachynema, and diplonema can be distinguished by the coimmunostaining patterns of SYCP3 and the phosphorylated form of histone H2AX (γH2AX) that marks DSBs formed during meiosis. Under normal conditions, γH2AX signals in lepSCs and zygSCs are spread throughout the nucleus, indicating large numbers of unrepaired DSBs. In contrast, in pacSCs and diplotene spermatocytes (dipSCs), the signals are constrained in the XY body. The clearance of γH2AX from the nuclei of pacSCs (except for the sex bodies) indicates that DSBs in the autosomes have been repaired (*13*). pacSCs were easily identified in WT testes by the costaining of γH2AX and SYCP3, but they were absent in the KO testes (Fig. 3A). In contrast, only lep/zygSCs were noted in the tubules of KO testes. Moreover, the total number of lep/zygSCs was much higher in KO testes than in WT testes (Fig. 3B and fig. S3A). These results indicated that meiotic DSBs were formed but not properly repaired in *Bend2* KO mice.

Coimmunostaining of SYCP3 and γH2AX was also carried out on surface-spread spermatocytes to reveal details. While all spermatocytes from leptonema to diakinesis of meiosis I were observed

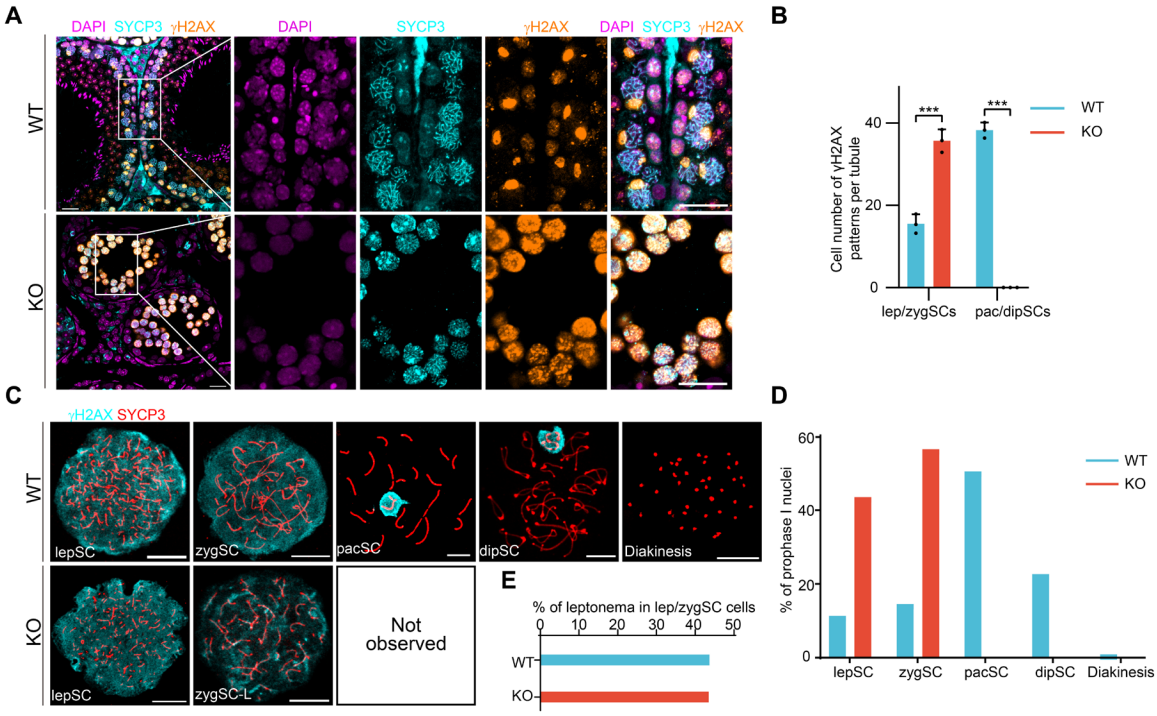

Fig. 3. Spermatocytes with *Bend2* KO fail to complete meiotic prophase. (**A**) Immunofluorescent labeling of testicular sections with mouse polyclonal SYCP3 antibodies (cyan) and rabbit polyclonal γH2AX antibodies (orange). DNA was counterstained with DAPI (magenta), and merged images are shown. Scale bars, 10 μm. (**B**) Average number of spermatocytes with γH2AX expression patterns per tubule. At least 100 tubules of each mouse were counted (***$P < 0.001$). (**C**) Nuclear spreads of various spermatocytes in WT and KO mice. Spermatocytes were immunostained with SYCP3 (red) and γH2AX (cyan). Scale bars, 10 μm. (**D**) Frequency statistics for spermatocytes in the meiotic prophase I stage for WT and KO mice. Number of spermatocytes analyzed: for WT, $n = 256$; for KO, $n = 180$. (**E**) Proportions of lepSC in lep/zygSC cells.

in WT testes, pacSCs with γH2AX signals constrained in the XY body and subsequent cell types were never observed in KO mice (Fig. 3C and fig. S3B). Moreover, the SYCP3-labeled chromosomal axes in KO zygSCs were not typical of the long continuous threads in WT zygSCs; rather, the former were more condensed, and we therefore named them zygSC-like cells (zygSC-LCs). Quantitative analyses showed that the percentages of lepSCs and zygSC-LCs among all cells at prophase of meiosis I were much higher in KO testes (Fig. 3D). As the diminution in the total number of spermatocytes contributed to the increase in the percentages of lepSCs and zygSC-LCs in KO testes, we calculated the percentages of lepSCs among lep/zygSCs and found that the percentage did not change between KO and WT mice (Fig. 3E). This suggested that the absolute number of lepSCs was increased in KO mice because the total number of cells with γH2AX staining per tubule was increased.

The progression of synapsis between homologous chromosomes can be monitored by the costaining of SYCP3 and SYCP1. Under normal conditions, SYCP3, but not SYCP1, can be detected in lepSCs; SYCP1 is initially detectable in zygSCs as short segments along the relatively more continuous SYCP3 threads, and it then becomes fully colocalized with SYCP3 to form the thick, smooth, and individualized synaptonemal complex in pacSCs. Unexpectedly, we noted SYCP1 in approximately 29% of KO lepSC-like cells (lepSC-LCs) (Fig. 4A), and we identified three types of zygSC-LCs (zygSC-L1, 46%; zygSC-L2, 28%; zygSC-L3, 26%) in KO testes (Fig. 4B). SYCP1 signals were primarily observed as small dots in zygSC-L1, while in zygSC-L2, they were thick or thin segments that represented the synaptonemal complex between homologous chromosomes and sister chromatids, respectively. In zygSC-L3, the SYCP1 signal was mostly detected as 40 discontinuous thin segments representing 40 univalents that underwent synapsis between sister chromatids.

Notably, SYCP3 signals in the form of forks, bubbles, and unequal branches were frequently detected in zygSC-L1 (Fig. 4B). The presence of multiple and unequal branches was more evident in images from superresolution structured illumination microscopy (SIM) and signified synapses between nonhomologous chromosomes (Fig. 4C and fig. S4A). Of interest, we found that HORMAD1 was highly enriched on axes when intersister synapsis occurred (fig. S4B). These results suggested that synapses initiated prematurely in KO mice (as early as in lepSC-LCs) but could not be fully established between homologs; instead, they progressed in incorrect directions to form nonhomologous and intersister synapses in different zygSC-LCs. As intersister synapsis was first uncovered in mice with cohesin gene *Rec8* KO and that was also observed in KO/mutant mice with several other cohesin genes, we examined whether REC8 foci were modified in *Bend2* KO mice (*14*). Because the REC8 foci were numerous and not well separated from each other, we measured the distances between well-separated foci along chromosomal axes in zygSCs and zygSC-LCs and found that the average distance in KO mice was significantly longer than that in WT littermates, suggesting a reduced number of REC8 foci in zygSC-LCs (Fig. 4D and fig. S4C).

Meiotic DNA DSBs are repaired in a stepwise manner. The DNA ends of DSBs are resected into long single-stranded 3′ overhangs that are initially coated by replication protein A (RPA) complexes. RPAs are subsequently replaced by the recombinase proteins RAD51 and DMC1 to form nucleoprotein filaments that seek a homologous template

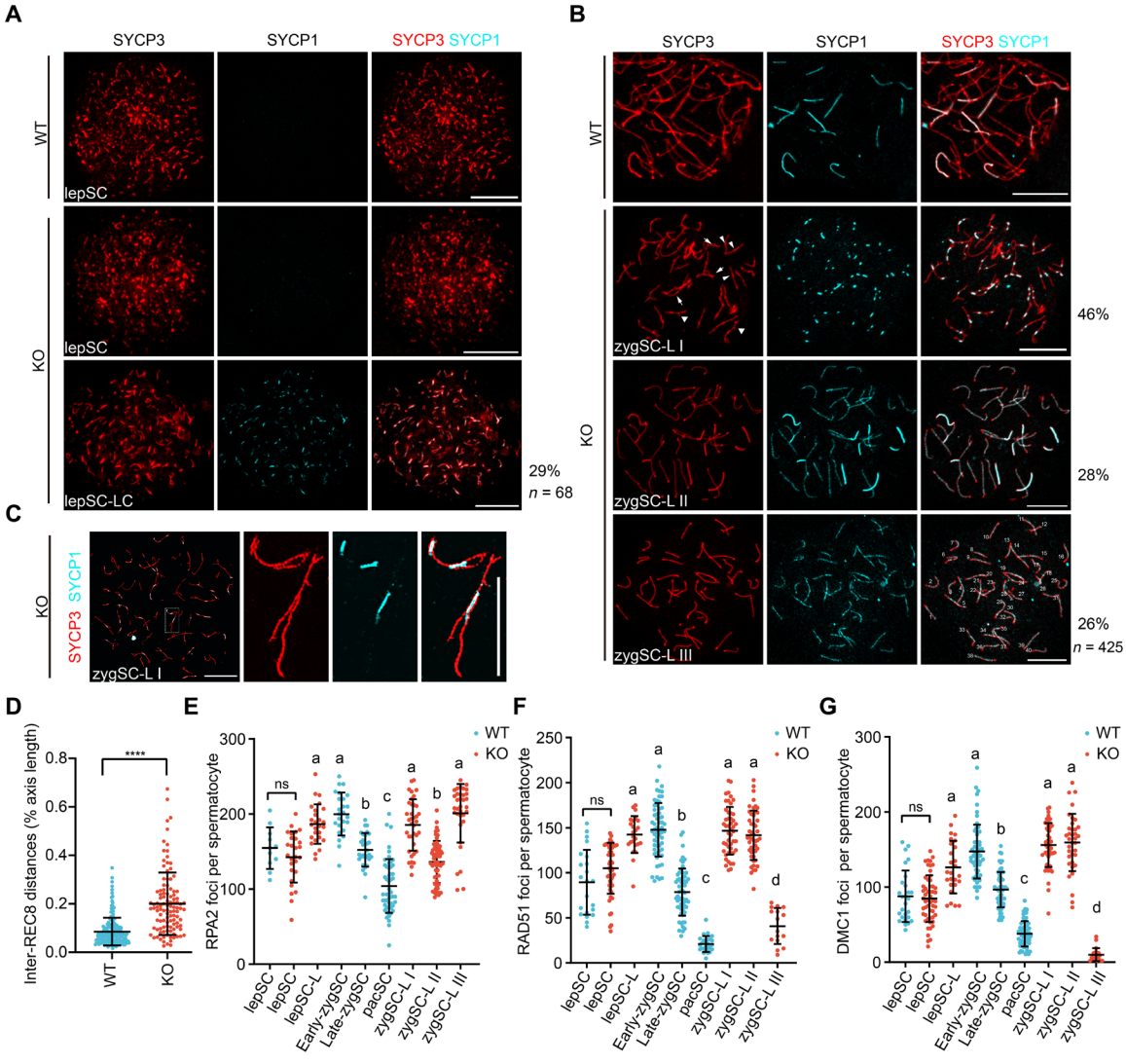

Fig. 4. BEND2 is required for homologous synapsis in meiosis. (**A** and **B**) Immunofluorescent labeling of SYCP3 (red) and the transverse filament protein SYCP1 (cyan), a marker of synapsis. (A) Abnormal SYCP1 signals were observed in lepSCs of KO mice compared with WT mice. Approximately 30% of lepSCs were abnormal in KO mice ($n = 68$). Scale bars, 10 μm. (B) SYCP3 and SYCP1 staining of WT zygSCs and KO zygotene-like spermatocytes. According to their staining with SYCP1 and SYCP3, zygotene-like spermatocytes were divided into three classes: zygSC-L I, 46%; zygSC-L II, 28%; and zygSC-L III, 26% ($n = 425$). Scale bars, 10 μm. (**C**) Superresolution microscopic images of zygotene-like spermatocytes showing abnormal synapsis. Scale bars, 10 μm. (**D**) Scatterplot in which we compared inter-REC8 distances along chromosomes in WT and KO mice (****$P < 0.0001$, obtained with two-tailed, unpaired t test). (**E** to **G**) Each dot represents the number of RPA2, RAD51, and DMC1 foci per spermatocyte; solid lines show the mean and SD of focus number in each group of spermatocytes. Data were analyzed using one-way analysis of variance (ANOVA) and Tukey's multiple comparison post hoc test; columns with different letters indicate a statistically significant difference ($P < 0.05$).

and form the recombinant intermediate, and are finally resolved into either crossovers between homologs or noncrossovers (*15*). We distinguished the DNA-bound RPA2, RAD51, and DMC1 as hundreds of foci along the SYCP3 threads in lepSCs and zygSCs by coimmunostaining (fig. S4, D to F). In WT mice, the focus numbers of all three proteins increased from leptonema to early zygonema, decreased from early to late zygonema, and reached their nadirs at pachynema (Fig. 4, E to G). The numbers of foci for RPA2, RAD51, and DMC1 were similar between the WT lepSCs and the normal-appearing KO lepSCs but were elevated to the levels of WT early zygSCs in the KO lepSC-LCs. The numbers of RPA2 foci in zygSC-L1 and zygSC-L2 were similar to those in early and late zygSCs in WT mice, respectively. Notably, the number of RPA2 foci in zygSC-L3 was also similar to that in early zygSCs, and the numbers of both RAD51 and DMC1 foci were similar among early zygSCs, zygSC-L1, and zygSC-L2. Of greater interest, the number of RAD51 foci in zygSC-L3s was lower than in late zygSCs but higher than in pacSCs, while the number of DMC1 foci in zygSC-L3 was the lowest among all cell types. These results suggested that lepSC-LCs were at a stage between leptonema and early zygonema and that zygSC-L1 and zygSC-L2 were likely to be in early zygonema (with aberrant formation and/or resolution of recombination intermediates), while zygSC-L3 might have been at late zygonema and undergoing intersister synapsis [but the latter's underlying mechanism(s) remains to be explored].

BEND2 interacts with transcriptional suppressors

As BEN proteins were predicted to mediate protein-protein and protein-DNA interactions, and since supportive evidence has been acquired for several family members, we next applied coimmunoprecipitation MS (co-IP–LC-MS/MS) to identify potentially interacting partners of BEND2. Co-IP was conducted using mmAb-FLAG to pull down FLAG-BEND2 and its interacting partners from testicular lysates from FLAG-BEND2 KI mice, and testicular lysates from WT mice were used as negative controls. By analyzing proteins enriched in FLAG-BEND2 KI samples in three independent experiments, we identified several potential BEND2-interacting proteins (Fig. 5A).

FLAG-BEND2 manifested the highest enrichment rank among all enriched proteins, indicating that our method was reliable. The next top three most significantly enriched proteins were ZMYM2, ADNP, and KDM1A (also known as LSD1). ZMYM2 is a member of the MYM (myeloproliferative and mental retardation)–type zinc finger protein family that contains six members in the human and mouse genomes (*16*). LSD1 is the first histone demethylase to be found and removes methyl groups from H3K4me or H3K4me2 (*17*). ZMYM2 has been identified as a component of LSD-containing repressive complexes, including the nucleosome remodeling and histone deacetylase (NuRD) complex (*18*). These complexes typically also contain histone deacetylases such as HDAC1 and HDAC2 that act upstream of LSD1 (*19*). Intriguingly, we found that HDAC1 and HDAC2 were enriched 1.6- and 1.2-fold, respectively, in our FLAG-BEND2 KI samples (table S1). ADNP is a transcription factor that contains nine zinc fingers and a homeobox domain, and is essential for embryonic and brain development (*20*). It was reported that ADNP, chromatin remodeler CHD4 (which is the motor component of the NuRD complex), and chromatin architectural proteins HP1β and HP1γ formed a stable complex named ChAHP that represses the expression of lineage-specifying genes in mouse embryonic stem (ES) cells (*21*). CHD4 consistently ranked number 7 in the list of BEND2-interacting proteins based on our results. Other potential interacting proteins that have been uncovered include TAF1B, GTF2H1, and PIWIL2.

The interactions of BEND2 with ZMYM2, ADNP, LSD1, CHD4, HDAC1, and HP1γ were confirmed by co-IP Western blotting results using the testicular lysates from FLAG-BEND2 KI mice (Fig. 5B). As positive controls, the interactions between CHD4 and HDAC1, HP1γ, or ADNP in the testis were also confirmed by our experiments (Fig. 5, C and D). We found that CHD4 was abundantly expressed in the nuclei of type A spermatogonia (SG-A) and weakly expressed in the nuclei of lepSCs, zygSCs, pacSCs, and dipSCs as granules similar to the pattern for BEND2 (fig. S5). In *Bend2* KO mice, the numbers of bright foci for CHD4 in lepSCs and zygSC-LCs were markedly reduced (Fig. 5E). By mining the human protein–protein interaction (PPI) data generated using the yeast two-hybrid technique (*22*), we also found that

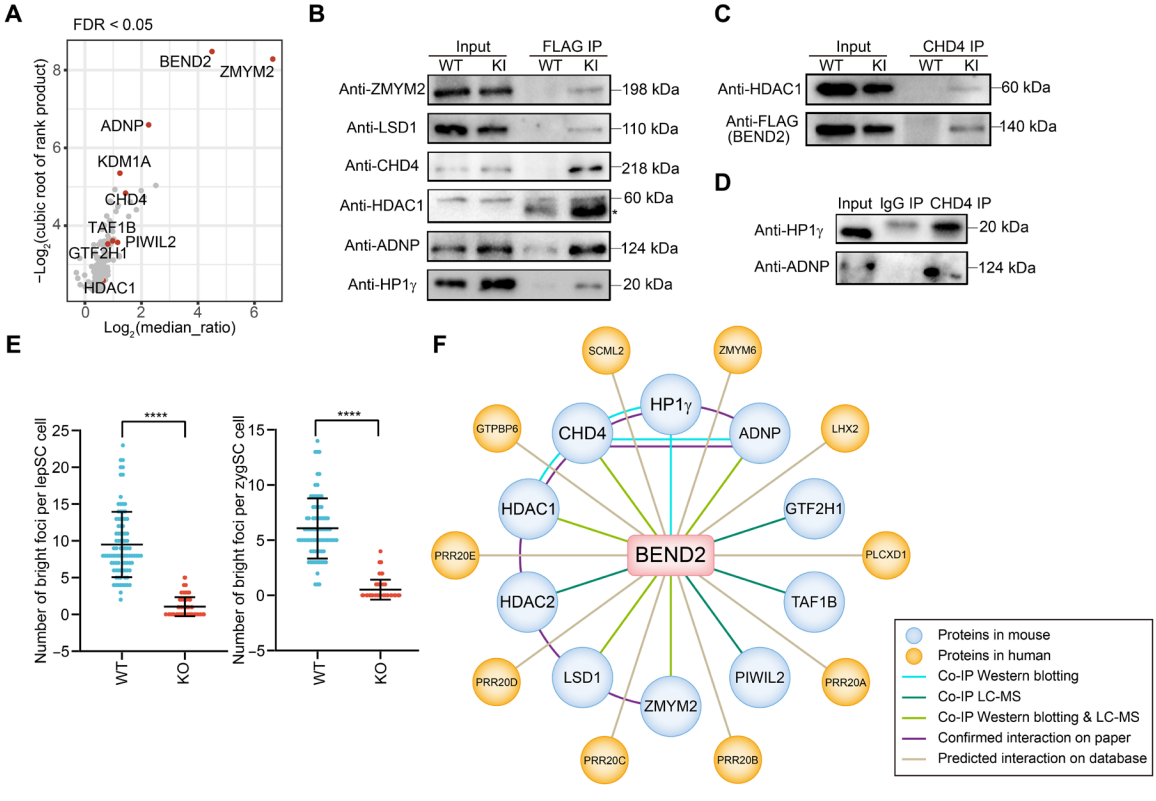

Fig. 5. MS analyses of BEND2-interacting factors in testicular extracts. (**A**) LC-MS/MS analysis of enriched protein from co-IP. Protein identification was performed in the presence of wash buffer containing 300 or 500 mM NaCl; WT mice served as background controls ($n = 3$ independent biological replicates, with each replicate containing two d-15 mice). (**B**) Co-IP of BEND2 with ZMYM2, LSD1, CHD4, HDAC1, ADNP, and HP1γ in testis from WT and *Bend2*$^{FLAG/Y}$ mice. The asterisk-labeled band is the heavy chain of mouse IgG. (**C**) Co-IP Western blot analysis used to confirm the interaction of CHD4 and BEND2 or HDAC1 in the testis. (**D**) Co-IP Western blot analysis to confirm the interaction of CHD4 and HP1γ or ADNP in the testis. (**E**) Each dot represents the number of bright foci per spermatocyte in WT and KO mice (****$P < 0.0001$, obtained with a two-tailed, unpaired *t* test). (**F**) Network of BEND2-interacting proteins.

human BEND2 might interact with ZMYM6, LHX2, SCML2, GTPBP6, and PRR20A-E. Therefore, BEND2 appears to interact with a large number of chromatin-binding proteins that are epigenetic regulators and/or transcription factors (Fig. 5F).

BEND2 preferentially binds to simple sequence repeats

To characterize BEND2-binding sites on the genome, we conducted chromatin immunoprecipitation sequencing (ChIP-seq) analyses by using testicular lysates from FLAG-BEND2 KI mice, and on the basis of the data from six independent experiments, a total of 16,477 peaks were identified (Fig. 6A; fig. S6, A to C; and table S2), and some peaks were validated by ChIP-PCRs (fig. S6D). Notably, BEND2 peaks were enriched in proximal promoters (from −1 kb to +100 bp of transcriptional start sites), CpG islands, 5′ untranslated regions (5′UTRs), and repetitive sequences ($P < 0.05$) (Fig. 6B and fig. S6E). Almost all peaks (95%) were localized to the intergenic regions (58%) and introns (37%), and these peaks were enriched in simple repeats, low-complexity sequences, and satellites (Fig. 6B and fig. S6E). The order of enrichment-fold values (ratios of observed-to-expected peak numbers) for the enriched genomic regions was simple repeats (15.9), low-complexity sequences (11.0), CpG islands (2.2), satellites (1.8), 5′UTRs (1.7), and promoters (1.3). We were interested in whether BEND2 peaks were enriched with any known or novel motifs, and noted that several similar GA-rich motifs were enriched in BEND2 peaks (Fig. 6C and fig. S6F). The top enriched motif (AGGAC/T/AAGGAC/T/AAG) was present in 44% of peaks ($P = 1 \times 10^{-5036}$) (Fig. 6C, left), and the average intensity (566 reads per peak) of peaks containing the top motif was 2.5-fold higher than that of peaks without the motif ($P = 1 \times 10^{-267}$). When we further conducted motif enrichment analyses on peaks that contained the top motif, we identified a similar top motif (AA/CG/CGAAAGGAA/TA) and several others (Fig. 6C, right, and fig. S6F). We observed that this top motif was similar to the motif for UME1, a protein that associates with histone deacetylases to repress meiotic gene expression during vegetative growth in yeast (*23*), and to the motif for PU.1, a well-known master regulator and pioneer factor in hematopoiesis from the ETS transcription factor family (*24*).

BEND2 binds to multiple chromatin states

We were interested in discerning how BEND2 sites in the mouse genome were related to different epigenetic markers such as histone modifications. Spruce *et al.* (*5*) recently defined an 11-state epigenomic map of lepSCs and zygSCs by using ChromHMM model based on ChIP-seq of 10 histone modifications. We reproduced the 11-state map and further annotated the map with more genomic features (RefSeq Genes, CpG islands, and repetitive sequences) and the binding

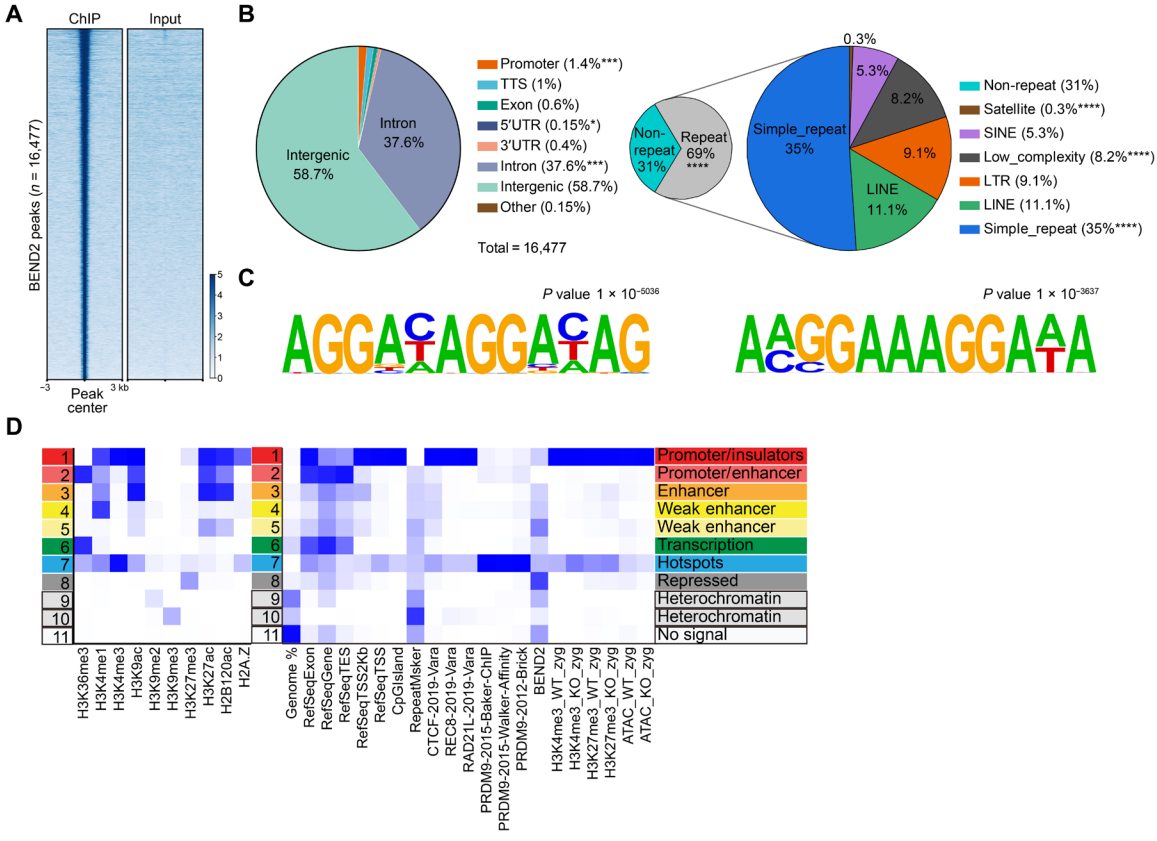

Fig. 6. BEND2 binds to multiple chromatin states. (**A**) Heatmap of BEND2 ChIP-seq enrichment across all peaks ($n = 16,477$) in the mouse genome. Each row represents a 6-kb window centered on BEND2 peak midpoints, sorted by the BEND2 ChIP signal. Input signals at the same position are shown on the right (average peak intensity of $n = 6$ biological replicates). (**B**) BEND2-binding sites were classified by their genomic locations and repeat types as indicated. (**C**) Top BEND2 DNA binding motif predicted by HOMER (left); sequences with the top motif reanalyzed by HOMER (right). (**D**) Heatmap of chromatin states produced by ChromHMM based on 10 histone modifications (left); heatmap showing different enrichment for indicated annotations for each state (right).

sites of proteins involved in meiosis (PRDM9, REC8, RAD21L, and CTCF) (Fig. 6D). Consistent with what Spruce *et al.* (*5*) found using a single dataset, we found that PRDM9 sites from three independent datasets were mostly enriched in state 7 (recombination hotspots), which is characterized by the moderate-to-high levels of H3K4me3, H3K36me3, H3K4me1, and H3K9ac. REC8, RAD21L, and CTCF were most enriched in state 1, which represents promoters and insulators, and second most enriched in hotspots. We also mapped BEND2 sites to the state map (Fig. 6D). BEND2 was notably enriched in multiple states, with the highest enrichment in state 8; this is typical of H3K27me3, which is a marker for the Polycomb repressive complex–repressed region. BEND2 was slightly enriched in state 1, which was annotated as promoters/insulators. These data suggest that BEND2 is involved in multiple functions in meiosis, one of which might be transcriptional suppression.

BEND2 regulates the expression of a large number of genes

We next executed RNA-seq analyses to identify differentially expressed genes (DEGs) upon *Bend2* KO in adult lepSCs and zygSCs that were isolated by fluorescence-activated cell sorting (FACS) (fig. S7, A to C). We identified 653 up-regulated and 2171 down-regulated DEGs in KO lepSCs as well as 685 up-regulated and 1607 down-regulated DEGs in KO zygSCs. For convenience, these four sets of DEGs were named lep-up, lep-down, zyg-up, and zyg-down, respectively. Notably, 59% (364 of 615) of the lep-up and 56% (364 of 654) of zyg-up sets overlapped with one another, and 54% (1057 of 1940) of the lep-down and 75% (1057 of 1403) of zyg-down sets overlapped with each other (Fig. 7, A and B; fig. S7D; and table S3). These results showed that lepSCs and zygSCs shared a high proportion of DEGs. The Gene Ontology (GO) terms enriched in the lep-up and zyg-up sets were similar (Fig. 7C and fig. S7E). For example, the top significantly enriched GO terms rated by false discovery rates (FDRs) from each set were "transcription," "cell cycle," "sterol biosynthetic process," "regulation of transcription," and "piRNA metabolic process" for lep-up, and "cell cycle," "transcription," "cell division," "regulation of transcription," "sterol biosynthetic process," "piRNA metabolic process," and "G1/S transition of mitotic cell cycle" for zyg-up. Some of these lep/zygSC up-regulated genes (*Dazl*, *Lin28a*, *Wdr81*, *Msh2*, *Kit*, *Mov10l*, *Piwil2*, *Stra8*, *Sohlh1*, *Src*, *Sohlh2*, and *Trip13*) were annotated as "germ cell development" or "oogenesis" (table S3). The GO terms enriched in the lep-down and zyg-down sets were also highly similar. The top five enriched GO terms in each set were "spermatogenesis, sperm motility, cell differentiation, cilium movement, and multicellular organism development" for lep-down and "spermatogenesis, sperm motility, cell differentiation, cilium movement, and spermatid development" for zyg-down (Fig. 7C and fig. S7E).

We also isolated pooled lepSCs/zygSCs from mice 12 days after birth (d12) to execute RNA-seq analysis as we posited that these cells that represented lepSCs and early zygSCs in the first wave of spermatogenesis (*25*) were more similar between KO and WT mice, and that DEGs identified using these cells contained fewer, if any, false-positive DEGs due to unmatched cell types (fig. S7, A and B). We identified 1267 up-regulated (d-12-up) and 796 down-regulated (d-12-down) DEGs between the KO and WT samples (table S5). Significantly enriched GO terms (FDR < 0.05) in the d-12 up-regulated gene set included those observed in the adult up-regulated gene sets, such as "cell cycle," "regulation of transcription," "mRNA processing," and "RNA splicing," while only three GO terms—"multicellular organism development," "intracellular signal transduction," and "cell differentiation"—were enriched in the d-12 down-regulated set (fig. S7E).

We next examined the expression dynamics of our DEGs using published sequencing data that included lep/zygSCs. We used the data from da Cruz *et al.* (*26*) that were generated from highly purified spermatogenic cells (particularly lep/zygSCs), using FACS, and data from Zhang *et al.* (*27*) that were generated by using cells purified with the traditional STA-PUT device. The da Cruz data comprised cell types that included lep/zygSCs (LZ), pacSCs (PS), round spermatids (RS), and mixed somatic cells and spermatogonia (2C), while the Zhang data entailed SG-A, plpSCs, lep/zygSCs, and pacSCs. Both the adult and d-12 up-regulated genes were expressed in SG and reached their zeniths in either LZ or plpSCs (fig. S7F), while the down-regulated genes peaked in RS or pacSCs. We also plotted the dynamics of single genes such as *Dnmt1*, *Dnmt3b*, *Lin28a*, *Dazl*, *Dmrt1*, and *Atm* and found that the patterns of single genes matched the average for all genes (fig. S7G). The expression changes in these and additional genes were validated by qRT-PCR (fig. S7H).

We next investigated whether BEND2 regulated gene expression by affecting chromatin accessibility and/or modifications. As meiosis in KO mice is arrested at zygonema, we isolated zygSCs from adult mice (2 months after birth) to implement assay for transposase-accessible chromatin using sequencing (ATAC-seq) and H3K4me3 and H3K27me3 CUT&RUN analyses and to compare differences in the distributions and intensities of the three signals between WT and *Bend2* KO samples (fig. S7I). From the ChromHMM state map, we observed that all three types of peaks in both WT and KO mice were mostly enriched in promoters followed by hotspots (states 1 and 7) (Fig. 6D). We did not note any changes in their global enrichment patterns by *Bend2* gene KO from the state map. However, by examining the signal intensities around transcription start sites (TSSs), we observed that ATAC-seq signals were enhanced in a large number of genes (clusters 1 and 2 versus cluster 3) in KO mice (Fig. 7D and fig. S7, J and K), and the H3K4me3 but not H3K27me3 signals were also enhanced in clusters 1 and 2 (Fig. 7E and fig. S7L). When we assessed whether up- or down-regulated genes in zygSCs based on RNA-seq were enriched in any of these three clusters, we found that only the up-regulated genes were enriched in clusters 1 and 2 ($P = 7.0 \times 10^{-3}$ and 3.6×10^{-11}, respectively) (Fig. 7F). Therefore, it appeared that gene repression by BEND2 was achieved by its contribution to maintaining low levels of chromatin accessibility and H3K4me3.

Last, we carried out luciferase assays to examine whether BEND2 suppressed gene expression by binding to genomic regions identified by the ChIP-seq analyses (Fig. 7, G and H). We first synthesized a DNA fragment containing five copies of the GGAAA consensus motif and inserted it upstream of the basal promoter of the luciferase-expressing plasmid. Intriguingly, the 5xGGAAA sequence enhanced the promoter activity by itself, and BEND2 enabled this enhancement to revert to basal levels. On the basis of the ChIP-seq data, we next tested several putative native BEND2-binding sites that were located either around the TSS (*Suz12*, *Lin28a*, and *Dmrt1*) or in the gene body (*Exo1*) of genes that were up-regulated in *Bend2* KO mice, and we observed that the overlapping or nearby ATAC-seq and H3K4me3 peaks were also up-regulated in KO mice. BEND2 significantly reduced the activities of three of the four putative binding sites (*Suz12*, *Lin28a*, and *Exo1*), regardless of whether the sites by themselves augmented or attenuated the activity of the basal promoter in the luciferase plasmid (Fig. 7H). These results further supported the

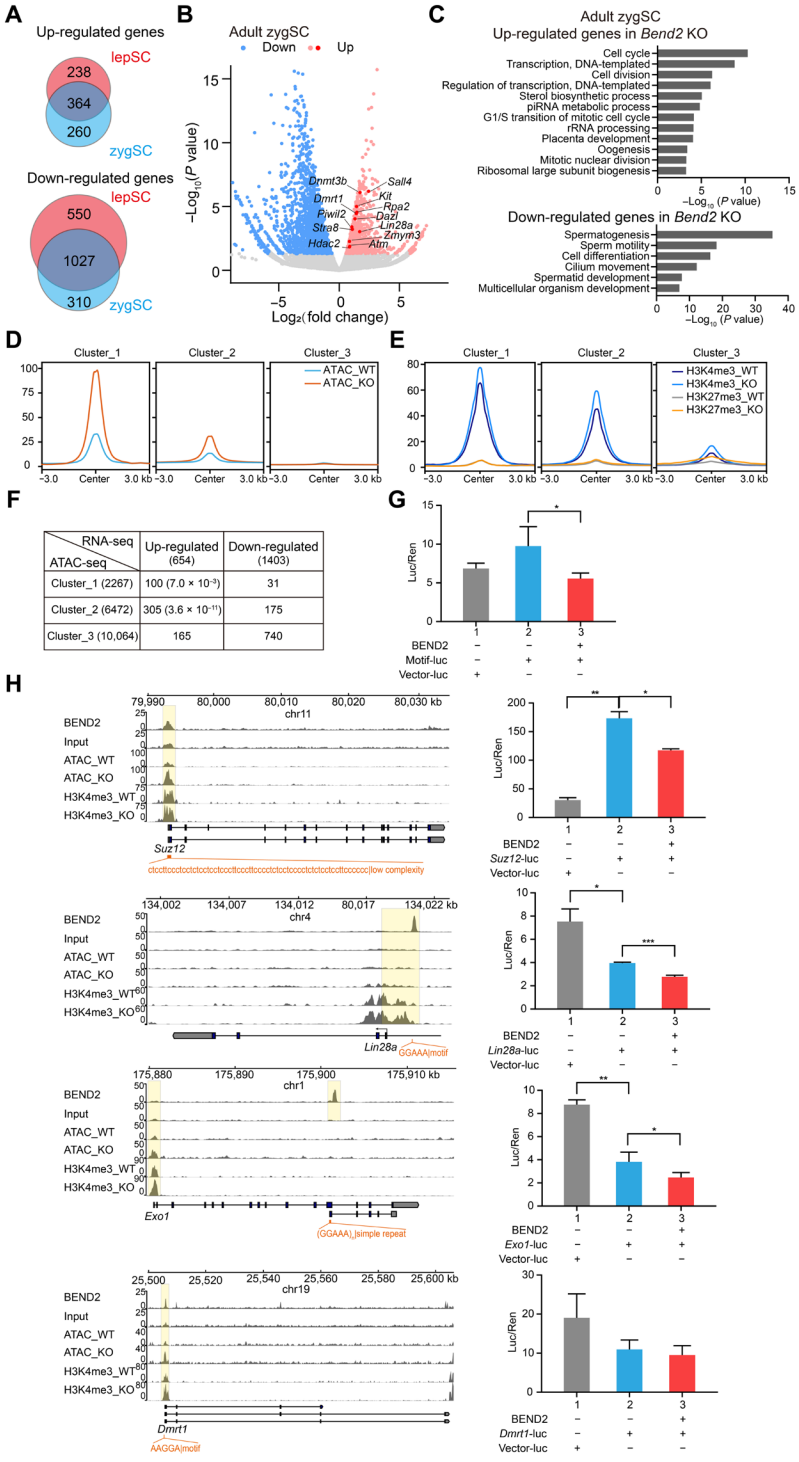

Fig. 7. Transcriptomic and epigenetic states change after *Bend2* KO. (**A**) The number of up- and down-regulated genes in lep/zygSCs of adult KO mice. The DEGs listed in the tables include both annotated genes with regular gene symbols and unannotated genes with only gene IDs, and only annotated genes were used to perform comparisons between different sets; the numbers of DEGs in the tables are therefore different from those indicated by the Venn diagrams. (**B**) Volcano plot of transcript levels between cells from adult WT and KO mice using zygSCs. The DEGs are highlighted in red (up-regulated in KO mice) and blue (down-regulated in KO mice). (**C**) Representative Gene Ontology (GO) terms of the biological process categories enriched in DEGs of zygSCs. (**D**) Average distribution of ATAC-seq signal around the TSS of three clusters of genes. (**E**) Average distribution of H3K4me3 and H3K27me3 around the TSS of three clusters of genes. (**F**) Correlation analysis between the three clusters of genes by ATAC-seq and DEGs. (**G**) Validation of DNA binding motif of BEND2 using dual-luciferase assay. *$P < 0.05$. (**H**) Browser view showing BEND2 ChIP-seq, ATAC-seq, and H3K4me3 ChIP-seq signals of target genes (left). Different types of peaks were first related to specific genes, and we noted gene sets associated with the different peaks as being of interest; genes at the intersection of all the sets were then selected to construct the track views. Track views of several genes involved in spermatogonial differentiation and meiosis were ultimately selected to represent the different types of peak localizations. Dual-luciferase assay showing the repression of BEND2 target genes ($n = 3$, **$P < 0.01$; right).

concept that BEND2 functions as a transcriptional suppressor of certain genes by binding to and modifying the chromatin accessibility and histone modifications of particular genomic regions.

DISCUSSION

Meiosis is a highly complex process that entails numerous concurrent or sequential steps that must be coordinated by a large number of regulators. In addition, investigators have in recent years repeatedly described novel regulators of meiosis using phenotypic evaluation of their gene KO mice via the highly efficient CRISPR-Cas9–based gene-editing technology. In the present study, we identified BEND2 as another previously unidentified regulator that is specifically expressed in male germ cells shortly before and after meiosis initiation, and is essential for DSB repair and synapsis. We also demonstrated that BEND2 interacts with other chromatin-binding/regulating proteins and regulates chromatin state and transcription. Our work has thus contributed another significant component to the arcane and complex physiologic process that is meiosis.

The BEN protein family was originally identified using bioinformatic analyses, and studies on this family are limited. BANP (BTG3-associated nuclear protein), also known as scaffold/matrix-associated region 1 (SMAR1) or BEND1, has been reported to act as both a tumor suppressor and an immunomodulator (*28*), and to repress cyclin D1 expression by recruiting the SIN3/HDAC1 complex to its promoter and to direct histone modifications from a distance (*29*). E5R is a virosomal protein from the chordopoxvirus subfamily and likely plays a role in organizing viral DNA during replication or transcription. NAC1 (nucleus accumbens–associated protein 1; also called NACC1 or BEND8) participates in various biological processes that include neuronal activity, pluripotency of ES cells, and tumor growth, and it interacts with HDAC3, HDAC4, and REST corepressor 1 (CoREST) (*30*). NAC1 was recently reported to bind DNA directly through the BEN domain in a sequence-specific manner (*31*).

BEND3 contains four BEN domains; is associated with HP1α, HP1β, HP1γ, and H3K9me3-containing heterochromatic foci; and represses transcription through interactions with HDAC1, HDAC2, HDAC3, and SALL4—a transcriptional repressor that also associates with the NuRD complex (*32*). In the absence of DNA methylation or H3K9me3 in mouse ES cells, BEND3 recruits the MBD3/NuRD complex to pericentromeric regions and is necessary for PRC2 recruitment and H3K27me3 establishment at major satellites, suggesting that it is a key factor in mediating a switch from constitutive to facultative heterochromatin (*33*). A recent study revealed that BEND3 was critical to maintaining H3K27me3 levels by stabilizing the PRC2 complex at bivalent genes in ES cells (*34*). BEND3 also represses ribosomal DNA (rDNA) transcription by interacting with the nucleolar remodeling complex and with Suv4–20h2, an enzyme responsible for H4K20 trimethylation (*35*). BEND5 and BEND6 contain a single BEN domain and are therefore (together with three fly proteins) called "BEN-solo" factors (*36*). BEND6, similar to its *Drosophila* homolog Insensitive, is most abundantly expressed in the brain and inhibits Notch target genes (*37*). BEND5 and the fly BEN-solo factors bind directly to specific DNA motifs through their BEN domains (*38*). BEND9 (NACC2 and RBB) recruits the NuRD complex to the internal promoter of HDM2 and inhibits the expression of HDM2, an E3 ligase that specifically targets p53 for ubiquitination and subsequent degradation (*39*). These studies on the BEN family members have indicated that BEN proteins are mostly key epigenetic regulators that interact with other proteins in DNA sequence-specific manners.

We have uncovered little information regarding BEND2, BEND4, and BEND7. Several studies showed that in-frame MN1-BEND2, EWSR1-BEND2, and CHD7-BEND2 gene fusions were detectable in brain and pancreatic neuroendocrine tumors (*40*–*42*). The current observations that all fusion partners of BEND2 are transcriptional regulators and that the fusion proteins maintain the BEN domain of BEND2 suggest that BEND2 probably binds DNA through its BEN domain.

As expected from the male germ cell–specific expression of *Bend2*, the KO mice displayed male infertility without any other overt phenotypes; this conclusion was solidly supported by the observation that all three types of mutant male mice ($Bend2^{-19/Y}$, $Bend2^{+1/Y}$, and $Bend2^{-4k/Y}$) were infertile. Detailed phenotypic evaluation was carried out with the $Bend2^{-4k/Y}$ males at and after F_2 (primarily at F_5 when the genetic background was purified to 98% of C57/BL6 by repeated crosses between $Bend2^{+/-}$ females and C57BL/6J males). Similar to the phenotypes manifested by mice with KOs of many other key meiotic regulators, *Bend2* KO mice exhibited arrested spermatogenesis at the zygonema/pachynema transition, with aberrant DSB repair and chromosomal synapsis. The manifestations of several defects imply molecular functions of BEND2 worth further investigation. First, synapsis initiation as marked by the appearance of SYCP1 signals was detectable in a significant portion (29%) of the KO lepSC-LCs, while it was rarely observed in WT cells. However, the formation of the invasive single-stranded DNAs essential for recombination and synapsis was basically not affected in the normal-appearing KO lepSCs as indicated by the numbers of RPA, RAD51, and DMC1 foci. In terms of the focus numbers for these meiotic proteins, zygSC-L1 and zygSC-L2 were likely to still be at early zygonema, while zygSC-L3 was at late zygonema and these cells show DSB repair disruption to varying degrees. However, DSB repair in zygSC-L3 may have progressed to D-loop formation with a sustained level of RPA2 when RAD51 and DMC1 were removed, or RAD51 and DMC1 were not stably assembled and thereby lost, resulting in the reloading of RPA. Although intersister repair may have also occurred here, we were unable to distinguish between these possibilities. Second, heterologous synapsis was noted in most meiotic mutants, with defects in the initiation or completion of meiotic DSB formation and repair. For example, nonhomologous chromosomal association has been reported in mice with KOs of a number of epigenetic regulators such as SUV39H, DNMT3L, and PRDM9 and was likely caused by the disrupted heterochromatin structure (*7*, *43*, *44*). Third, intersister synapses were common in our *Bend2* KO zygSCs, and either full or local intersister synapses were observed in cohesion-protein KO mice, including KOs of REC8, SMC1β, and STAG3 (*45*). REC8 foci were also consistently reduced in *Bend2* KO mice. The phenotypes of *Bend2* KO mice might therefore reflect those of different meiotic regulators, and this implies that BEND2 interacts with these regulators either physically or genetically or both.

One caveat to our study was that the lepSC-LCs we observed in the KO mice might have also represented nuclei at a late zygotene-like stage that included a fragmented synaptonemal complex. Xu *et al.* (*14*) similarly observed an abnormal costaining pattern of SYCP3 and SYCP1 in cells of *Rec8* KO mice, and they asserted that the cells were at leptonema. As the phenotype of *Bend2* KO and *Rec8* KO

mice was similar in terms of intersister chromatid synapsis, we hypothesized that *Bend2* KO lepSCs also underwent premature assembly of the synaptonemal complex as exemplified by their *Rec8* KO counterparts. Moreover, the hypothesis that lepSC-LCs were at leptonema when partial synapsis occurred prematurely was easier to comprehend than one in which these cells were at late zygonema after the synaptonemal complex was fragmented aberrantly following the formation of long synaptonemal complexes at early or mid-zygonema. It is more likely that lepSC-LCs represent an abnormal intermediate stage between leptonema and zygonema as indicated by the levels of RPA2, RAD51, and DMC1, which were similar to levels in early zygSCs of WT mice.

The first clue as to the molecular mechanism underlying BEND2 function in meiosis comes from the observation that it interacts with multiple proteins, of which most are transcriptional repressors that often interact with other BEND proteins. Most of these proteins (HDAC1, HDAC2, CHD4, LSD1, ZMYM2, HP1γ, and ADNP) are either core components or interacting proteins of two repressive complexes: the well-known NuRD complex (*46*) and the recently identified ChAHP complex (*21*). This observation, together with the fact that our co-IP washing solution contained 500 mM NaCl, suggested that the interactions between BEND2 and these complexes were fairly robust. The overlapping expression windows of BEND2 and CHD4, their similar granular expression patterns, and the reduced signal for CHD4 in *Bend2* KO mice also supported an interaction between these two proteins. As CHD4 has been shown to promote the repair of DNA DSBs and cellular survival in somatic cells (*47*, *48*), and since it interacts with BEND2, these observations facilitate the clarification of why and how meiotic DSB repair was disrupted in *Bend2* KO mice. However, whether CHD4 exerts a direct action in meiotic DSB repair remains to be established.

Moreover, the *Bend2* KO mice were similar to HP1γ mutants, as asynapsis and univalency of homologous chromosomes and heterophilic interactions of chromosomal ends were observed in the mice with KOs of both genes (*49*). The interactions we observed between these two proteins and their locations in various heterochromatin types were thus congruent with the aforementioned similarities. Other familiar interacting proteins of BEND2 that we identified in the present study included DNA binding proteins such as TAF1B, GTF2H1, and PIWIL2. PIWIL2 (also known as MILI) is one of three mouse PIWI subfamily proteins (MIWI, MIWI2, and MILI) that bind to Piwi-interacting RNAs (piRNAs), and is required for spermatogonial stem cell self-renewal, spermatogonial differentiation, and meiosis (with spermatogenesis ultimately arrested at the zygonema or early pachynema stage in KO mice), and PIWIL2 is localized to both cytoplasm and nucleus (*50*). A recent study provocatively showed that mice with a KO of the testis-specific protein TEX15 exhibited a similar meiotic arrest phenotype, that it was also both cytoplasmic and nuclear localized, and that it regulated the expression of retrotransposons through DNA methylation and a physical association with PIWIL2 (*51*). On the basis of our data and bioinformatic predictions from the PPI database, BEND2 interacts with many other proteins; however, the significance of these interactions is currently unclear. Nevertheless, these observations suggested that BEND2, like other family members, may be important in regulating chromatin activities such as heterochromatin formation/maintenance, transcription, and higher-order structure.

The potential regulatory roles of BEND2 with respect to chromatin are also supported by the distribution of its ChIP-seq peaks in various genomic regions and the chromatin states that are defined epigenetically. The observation that BEND2 did not robustly colocalize with chromocenter in spermatocyte compartments did not necessarily indicate that it localized to the euchromatic regions, as the resolution of our immunostaining method was not very high. To address this situation, we applied ChIP-seq analyses to provide improved genomic localization. The peaks were enriched in regulatory regions such as promoters, CpG islands, enhancers, recombination hotspots, and PRC-repressed sites. It was particularly interesting that the intronic and intergenic peaks (which comprised 96% of the total peaks) were highly enriched in simple repeats and low-complexity repeats, and that a GA-rich motif was also enriched in these peaks. Our ChromHMM results also revealed that BEND2 bound to multiple chromatin states, with its highest enrichment found in facultative heterochromatin. This is reminiscent of BEND3, which has been found to bind to pericentromeric chromatins of mouse ES cells in the absence of DNA methylation or H3K9me3, and it thereby constitutes a potentially redundant pathway for generating repressive chromatin (*33*).

The analyses of transcriptomic changes in spermatocytes of *Bend2* KO mice provided further clues regarding the molecular functions of BEND2 as a chromatin regulator. It appears that BEND2 suppresses genes that begin to undergo expression in spermatogonia and that attain their peak levels around the time of meiotic initiation. These BEND2-suppressed genes were shown to be involved in spermatogonial differentiation or meiotic initiation and/or progression (*26*), and a similar role for BEND2 would be consistent with its narrow expression window that spans cell types from SG-B to pacSC. Down-regulated genes in adult KO mice (i.e., genes activated by BEND2) may have contained more false positives, as late zygSCs were absent in the KO mice. It was also noteworthy that DEGs from adult and d-12 lep/zygSCs were not very similar, reflecting the concept that the first wave of spermatogenesis was different from subsequent waves; in this sense, results from d-12 and adult mice were complementary to each other. It will also be important to investigate BEND2's regulation of gene expression in an age-dependent fashion in the future.

An increasing body of evidence signifies that gene repression is an essential means of gene regulation in diverse cellular developmental processes. As far as germ cells are concerned, somatic genes are repressed in early-stage primordial germ cells in both sexes (*52*), while the meiotic program is prevented in male gonocytes and spermatogonia by the retinoic acid-metabolizing pathway and proteins such as NANOS2, DMRT1, and SCML2 (*9*, *53*, *54*). Thus, the identification of BEND2 as a repressive regulator indicates that this regulatory scheme may be much more extensive and complex than previously thought. Since a repressor can specifically activate the expression of genes as an indirect result of the repression of other repressors that target the activated genes, it is not surprising that a large group of genes involved in meiotic and postmeiotic activities of spermatogenic cells can be down-regulated upon *Bend2* KO. This suggests that BEND2 contributes to the expression of these genes under normal conditions, and among the genes normally repressed by BEND2 (up-regulated genes in *Bend2* KO mice), 36 were negative regulators of transcription according to their GO annotations (table S3). Important repressive regulators in this list include SALL1, SALL4, DNMT1, DNMT3B, SUV39H2, BEND3, and DMRT1; some of these were known to be of critical significance to spermatogonial

proliferation, differentiation, and meiotic initiation. For example, DMRT1 is a repressor of meiotic initiation as its KO in mice initiates meiosis precociously (*54*). PRC2, of which SUZ12 is a core subunit, is required for spermatogonial stem cell maintenance and meiotic progression via repression of somatic and meiotic gene expression (*55*). Moreover, we consistently showed with luciferase assays that the TSSs of both *Dmrt1* and *Suz12* contained BEND2-binding sites that were repressive in the presence of BEND2.

In summary, we identified BEND2 as a germ cell–specific regulator of meiosis with detailed examinations of its expression and function by using gene KI and KO mice. We also demonstrated the molecular mechanisms underlying BEND2's action as a chromatin modulator and transcriptional repressor by identifying and characterizing its interacting partners, genomic binding sites, and regulated genes. The aberrations in meiotic synapsis and DSB repair in our KO mice were very likely the result of multiple disturbances that included aberrant gene expression, aberrant chromatin structure, and reduced loading of key meiotic proteins. However, there are many more issues that await clarification in the future, for example, whether BEND2 is critical to female meiosis (oogenesis), whether it acts as a direct modulator of the meiotic machinery independent of its role in transcriptional repression, and whether molecular defects can be detected before meiotic initiation. Our present study will establish a solid foundation for future investigations.

MATERIALS AND METHODS

Mice

All animal procedures were approved by the Animal Ethics Committee of the Institute of Zoology, Chinese Academy of Sciences. All experiments with mice were conducted in accordance with the *Guide for the Care and Use of Laboratory Animals*. *Bend2* mutant mice were generated through the CRISPR-Cas9 gene-editing approach (*56*). One male and two female founder mice with DBA/2/C57BL/6J background were acquired by using different guide RNAs (gRNAs). For $Bend2^{-4k/Y}$ mice, we designed two gRNAs for the long-fragment deletion, while only one gRNA was designed for the generation of $Bend2^{+1/Y}$ and $Bend2^{-19/Y}$ mice. Genomic DNA extraction followed the standard proteinase K–chloroform method. Genotyping for $Bend2^{+1/Y}$ and $Bend2^{-19/Y}$ mice was executed by Sanger sequencing following PCR amplification, while two pairs of primers were designed for genomic identification of $Bend2^{-4k/Y}$ mice; p1 and p2 primers were used to identify the WT and KO allele, respectively (all primers are listed in table S5). *Bend2-3xFLAG* KI mice were generated through the CRISPR-Cas9 gene-editing approach. The targeting fragment was designed to insert 3xFLAG in-frame with the coding sequence just after the first ATG of the *Bend2* genomic locus. To ensure accuracy, we designed two gRNAs and compared their efficiencies: KI-gRNA-2 was more efficient and is listed in table S7. The donor DNA contained a 3xFLAG-Linker, with left and right homology arms (800 bp). Donor DNA was synthesized by Sangon Biotech. Our genomic DNA extraction followed the standard proteinase K–phenol/chloroform method. Genotyping was carried out with PCR, and the primers used are listed in table S5.

Bend2 cDNA clone

Total RNA was extracted from adult mouse testis, and reverse transcription was performed using the High-Capacity cDNA Reverse Transcription Kit (4368814, Applied Biosystems). We used nested PCR for the *Bend2* cDNA clone (two pairs of primers were designed, and their sequences are provided in table S5). The PCR products were purified with agarose gel electrophoresis and recovered with an EasyPure quick gel extraction kit (M2073, TransGen Biotech). The cDNA was cloned into a pGM-T plasmid (VT202-02, TIANGEN Biotech), and the cDNA sequence was identified by Sanger sequencing.

Antibody generation

An antibody to mouse BEND2 (rpAb-B2-1) was produced by ABclonal Technology (Wuhan, China) and generated by immunization of rabbits with the peptide sequence DVRESVKRERVDFEHT-PDANPEGSDNASIN-C (amino acids 585 to 614). For rpAb-B2-2, mouse *Bend2* cDNA (nucleotides 729 to 1458) was inserted in-frame into vector Pet42b to produce a fusion protein (BEND2-8x His) that consisted of N-terminal amino acids 243 to 486 of mouse BEND2 and eight tandem histidine residues. The fusion protein was expressed in *Escherichia coli* (strain BL21), affinity-purified with Ni-NTA (nitrilotriacetic acid) resin, and used to immunize rabbits. Antibodies were purified on an antigen affinity column.

Histological, immunohistochemical, immunofluorescence, and TUNEL staining in testicular sections

Testes or epididymides from WT and KO mice were dissected and fixed with Bouin's solution or 4% paraformaldehyde (PFA) and then embedded in paraffin and sectioned at 5 μm for staining. For H&E staining, Bouin's solution–fixed sections were stained with H&E following standard protocol. For immunofluorescence or immunohistochemical study, 4% PFA-fixed sections were dewaxed and rehydrated, and then slides were incubated with sodium citrate buffer (pH 6.0) at 95°C for 10 min to retrieve antigen. Five percent bovine serum albumin (BSA) or 5% skimmed milk was used to block nonspecific antigens for 1 hour at room temperature. Primary antibodies were diluted with 5% BSA and then incubated with sections at 4°C overnight. After washing three times with phosphate-buffered saline (PBS), diluted secondary antibodies conjugated with fluorescent tag or horseradish peroxidase (HRP) were incubated with sections. For immunofluorescence, DNA was stained with 4′,6-diamidino-2-phenylindole (DAPI) diluted by PBS, and photomicrographs were taken with confocal fluorescence microscopes (LSM780, Zeiss; LSM880, Zeiss; Nikon A1 N-SIM S, Nikon). For immunohistochemistry, a DAB (3,3′-Diaminobenzidine) solution as chromogen was diluted and used to cover the sections at room temperature for 10 min; this was immediately followed by PBS to stop the reaction. Slides were dehydrated, and nuclei were stained with hematoxylin. Images were taken with an optical microscope (ECLIPSE 80i, Nikon). We implemented the DeadEnd Fluorometric TUNEL System (G3250, Promega) for TUNEL staining. The seminiferous-epithelium cycle can be divided into 12 stages (I to XII) through developmental spermatocytes and spermatids (*57*). For WT testis sections, stages were recognized by the organization of spermatocytes and spermatids as visualized by hematoxylin staining. For KO testis sections, stages of seminiferous epithelium were only identified according to the types of spermatocytes because of the lack of spermatids.

Western blot analysis

Tissues were harvested and washed once with PBS. After mechanically shearing them into pieces, we transferred the tissues to a Dounce homogenizer in radioimmunoprecipitation assay lysis buffer (P0013B, Beyotime) containing protease inhibitor cocktail, and the mixture

was incubated on ice for 30 min. Cell debris was removed by centrifugation at 13,500*g* for 15 min at 4°C, and lysates were boiled with 5× SDS loading buffer for 10 min. Tissue extracts were electrophoresed on SDS-PAGE gels containing different concentrations of separation gels between 6 and 15% based on the molecular weights of the proteins and then blotted onto polyvinylidene difluoride membranes (88518, Thermo Fisher Scientific). Membranes were blocked with 5% skimmed milk for 1 hour at room temperature and then incubated in dilutions of primary antibodies overnight at 4°C. After washing three times with PBST (Phosphate Buffered Saline, 0.1% Tween 20), membranes were incubated in HRP-conjugated secondary antibodies (diluted in PBS) for 1 hour at room temperature, and the membranes were then washed three times with PBST at room temperature with gentle shaking. The protein blots were ultimately detected with SuperSignal West Pico Plus Chemiluminescent Substrate (34577, Thermo Fisher Scientific) and imaged on a Bio-Rad Universal Hood II imaging system.

Spermatocyte spreading and immunofluorescence staining

Testes were dissected from 2- to 4-month-old mice, and the seminiferous tubules were washed in PBS. The tubules were then placed in a hypotonic extraction buffer for 30 to 60 min. Subsequently, the tubules were minced in 0.1 M sucrose (pH 8.2) on a clean glass slide and pipetted repeatedly to create a cellular suspension; the suspensions were then spread on slides containing 1% PFA and 0.15% Triton X-100 (pH 9.2) and dried for at least 2 hours in a closed box with high humidity. Last, the slides were washed twice with 0.4% Photo-Flo 200 (Kodak), dried at room temperature, and stored at −80°C for immunofluorescent staining. Slides were equilibrated to room temperature, and then each was washed with PBS twice for 5 min with gentle shaking. BSA (5%) was dropped onto the slides for blocking, and they were covered by parafilm for 1 hour in a humidified box. Fluorescence staining was identical to that described for immunofluorescence staining. Immunolabeled nuclei with chromosomal spreads were imaged on confocal laser scanning microscopes (LSM780, Zeiss; LSM880, Zeiss) using a 63× oil-immersion objective. For SIM, images were taken on a Nikon A1 N-SIM S microscope. Images were processed using Imaris (v9.2.1) for focus analysis and Photoshop (Adobe) to construct the figures. We only counted foci that colocalized with the chromosomal axis.

Co-IP mass spectrometry

Four testes from *Bend2-3xFLAG* KI mice or WT mice were homogenized on day 15 by using Dounce homogenizers in 1 ml of cold lysis buffer [20 mM tris-HCl (pH 7.4), 150 mM NaCl, 1 mM EDTA, 5% glycerol, and 1% NP-40, with fresh 100× proteinase inhibitor added just before use] and then incubated on ice for 30 min. We removed cellular debris by centrifugation at 13,500*g* for 15 min at 4°C, and cell lysates were precleared with 25 μl of protein G beads (10003D, Invitrogen) at 4°C for 1 hour. For MS, 80 μl of Anti-FLAG Magarose Beads (SM00905, SMART LIFESCIENCES) was added to the precleared lysates and the mixture was rotated at 4°C overnight. The beads were washed four times with cold, low-salt co-IP wash buffer [20 mM tris-HCl (pH 7.4), 300 mM NaCl, 1 mM EDTA, 5% glycerol, and 1% NP-40, with fresh 100× proteinase inhibitor added just before use] or high-salt co-IP wash buffer [20 mM tris-HCl (pH 7.4), 500 mM NaCl, 1 mM EDTA, 5% glycerol, and 1% NP-40, with fresh 100× proteinase inhibitor added just before use], rotating each time for 15 min at 4°C. Proteins were eluted from the beads with 25 μl of 1× SDS loading buffer and boiled for 10 min. The presence of proteins in the immunoprecipitated samples was confirmed by SDS-PAGE using a 10% concentration of separation gel and silver staining. Whole samples collected from the gel were used to perform MS analyses. For co-IP Western blotting, 80 μl of precleared lysates mixed with 5× SDS loading buffer was boiled for 10 min as an input sample before immunoprecipitation. The other lysates were incubated with 5 μg of antibodies or isotype immunoglobulin G (IgG) as experimental samples and negative control, respectively, and rotated at 4°C overnight. We then added 30 μl of Dynabeads Protein A/G (10001D and 10003D, Invitrogen) to each sample based on the host species of the antibodies and incubated the samples at 4°C for 4 hours. The washing and elution steps were the same as described above. Proteins that potentially interacted with BEND2 were mined using two web tools—HuRI (The Human Reference Interactome, http://interactome-atlas.org/) and STRING (https://string-db.org/).

RNA sequencing

We collected spermatocytes from adult and d-12 mice via FACS. For adult mice, lepSCs and zygSCs were collected in accordance with previous methods (*58*). Briefly, the testes from one adult WT mouse or from three adult KO mice were digested by two-step methods. Seminiferous tubules were segregated with collagenase I and deoxyribonuclease (DNase) I, and then 0.25% trypsin and DNase I were used to obtain a single-cell suspension. Testicular cells isolated from WT and KO mice were then sorted by FACS after Hoechst 33342 staining. Different types of spermatocytes were then collected through Hoechst Blue and Hoechst Red channels. For d-12 mice, the testes from one WT or KO mouse were also digested using a two-step method as described above. The larger tetraploid cells in the testis were considered spermatocytes and sorted by FACS after Hoechst 33342 staining. RNA was prepared following the TRIzol (Invitrogen) protocol. All RNA libraries were constructed at the same time using the NEBNext Ultra Directional RNA Library Prep Kit for Illumina (E7760) according to the manufacturer's recommendations, and the NEBNext rRNA Depletion Kit (E7405) was used to delete ribosomal RNA (rRNA). Our RNA-seq analyses followed a standard procedure that included mapping sequence reads to the mouse genome mm10 using Hisat2 (hisat2-2.2.0) and identifying DEGs using the DESeq2 R package.

Chromatin immunoprecipitation sequencing

Approximately 60 mg of testicular tissues from mice at d15 or d40 was disaggregated by Dounce homogenization, and the chromatin was cross-linked in PBS containing 1% formaldehyde for 10 min at room temperature. Fixation of chromatin was halted with a 1.25 M glycine solution and washed three times with cold PBS. Cells were lysed for 30 min on ice by adding cell lysis buffer [50 mM tris-HCl (pH 8.0), 10 mM EDTA, and 1% SDS, and fresh 1 mM phenylmethylsulfonyl fluoride and protease inhibitor were added before use]. Chromatin was then sonicated for 20 s at 25% power in 30-s pulses for 20 cycles, cellular debris was removed by centrifugation, and the supernatant was precleared by IgG for 2 hours at 4°C. About $^{1}/_{20}$th of the chromatin was saved as an input sample, and the remainder was diluted to 10× volume with IP dilution buffer [20 mM tris-HCl (pH 8.0), 150 mM NaCl, 2 mM EDTA, 1% Triton X-100, and 0.01% SDS] and incubated with 10 μg of antibody for 2 hours at 4°C. Protein A/G (10001D and 10003D, Invitrogen) Dynabeads were added to capture targeted chromatin overnight. Beads were washed with a

four-step wash buffer [low-salt wash buffer, 20 mM tris-HCl (pH 8.0), 2 mM EDTA, 50 mM NaCl, 1% Triton X-100, and 0.1% SDS; high-salt wash buffer, 20 mM tris-HCl (pH 8.0), 2 mM EDTA, 500 mM NaCl, 1% Triton X-100, and 0.01% SDS; LiCl wash buffer, 10 mM tris-HCl (pH 8.0), 1 mM EDTA, 0.25 M LiCl, 1% NP-40, and 1% deoxycholic acid; TET buffer, 10 mM tris-HCl (pH 8.0), 1 mM EDTA, and 0.1% Tween 20]; beads were washed twice for each step. After the chromatin was eluted from the beads by elution buffer [10 mM tris-HCl (pH 8.0), 1 mM EDTA, and 1% Tween 20], cross-linking was reversed with 5 M NaCl at 65°C for 16 hours, and RNA and protein were digested by adding ribonuclease A and protease K for 2 hours at 37° and 45°C, respectively. Extracted DNA was used to construct a library with the NEBNext Ultra II DNA Library Prep Kit for Illumina (E7645, NEB), and qualified libraries were sequenced with an Illumina NovaSeq 6000 system to obtain paired-end 150-nucleotide (nt) reads.

CUT&RUN

We collected zygSCs from adult mice via FACS as described above, and CUT&RUN was primarily performed according to Henikoff and colleagues (*59*). In brief, before experimentation, 10 μl of concanavalin A beads (BP531, Bangs Laboratories) was washed twice with binding buffer, resuspended with 10 μl of binding buffer, and maintained on ice. For each sample, ~20,000 cells were suspended in wash buffer, incubated with prepared beads, and mixed for 10 min at room temperature. After discarding liquids, beads were incubated with antibody buffer on a Thermomixer at 4°C overnight. Beads were washed once with Dig-Wash buffer and resuspended with the same buffer containing pAG-MNase (700 ng/ml) that was purified according to methods described previously (*59*), and this mixture was then incubated for 3 hours at 4°C. Beads were then washed twice with the Dig-Wash buffer, resuspended in the same buffer containing 2 mM $CaCl_2$, vortexed, and placed on ice as soon as possible. After 30 min, a 2× stop buffer was added to quench the digested reaction, and it was incubated at 37°C for 30 min. The suspensions were collected, and the DNA was extracted. We prepared the library using the NEBNext Ultra II DNA Library Prep Kit for Illumina (E7645, NEB) and sequenced the qualified libraries with an Illumina NovaSeq 6000 system to obtain paired-end 150-nt reads.

Assay for transposase-accessible chromatin using sequencing

zygSCs were collected from adult mice by FACS as described in CUT&RUN, and cells were washed twice with cold PBS. To prepare nuclei, cells were lysed with cold lysis buffer [10 mM tris-HCl (pH 7.4), 10 mM NaCl, 3 mM $MgCl_2$, and 0.1% NP-40], maintained on ice for 10 min, and centrifuged at 500*g* for 5 min at 4°C. After carefully removing the suspension, we resuspended the pellet in the transposase reaction mix (TD501, Vazyme) and incubated it at 37°C for 10 min. Fragments were then immediately purified with 2× AMPure XP beads (A63881, Beckman), and library amplification was performed using the TruePrep DNA Library Prep Kit V2 for Illumina (TD501, Vazyme). Paired-end reads were aligned with Bowtie2 using default parameters, and only uniquely mapping reads were retained for further analysis; PCR duplicates and blacklist region reads were removed. Peak calling was executed using MACS2 (v2.2.7.1). Different gene clusters and heatmaps were then generated using the command-line version of deepTools (v3.5.0). The three gene clusters were defined arbitrarily with a *K*-means clustering method, and the *K* value was decided to be 3 based on visual inspection of the initial heatmap generated with the deepTools software. Correlation analysis of the three clusters of genes by ATAC-seq and DEGs was based on a hypergeometric distribution.

ChIP-seq and CUT&RUN analysis

ChIP-seq raw reads were trimmed to remove adapter sequences when converting them to a fastq file, and the trimmed ChIP-seq reads were mapped to the UCSC mm10 genome using Bowtie2 (v2.4.1) and default parameters. For BEND2, peak calling was performed using Pepr with default parameters and the corresponding inputs as background, and peaks that mapped to blacklist (*60*) regions were removed. Annotation of genomic locations and repeat types was generated using HOMER (v4.11), and heatmaps were generated using the command-line version of deepTools (v3.5.0). Reproducibility of replicates was calculated with read densities in 5-kb bins across the entire genome by deepTools, and scatterplots were plotted with plotCorrelation using the Pearson method. Distributions of BEND2-binding sites on the chromosomes were generated by ChIPseeker (v1.24.0), and HOMER (v4.11) was applied with default settings to identify enriched motifs in the BEND2 peaks. For CUT&RUN, we generated distributions of three different gene clusters and heatmaps using the command-line version of deepTools (v3.5.0). RepeatMasker and TSS-location files were downloaded from the UCSC website, and we achieved a Genome Browser view of the next-generation sequencing data by using the command-line version of pyGenomeTracks.

Luciferase assay

Bend2 cDNA was cloned into a pFLAG-CMV-4 vector, and the BEND2-targeted regions for *Dmrt1*, *Suz12*, *Lin28a*, and *Exo1* were PCR-amplified from mouse genomic DNAs isolated from mouse tail tips and cloned into a PGL4.23-luciferase vector (Promega, E8411). Five copies of a GGAAA sequence were synthesized by Sangon Biotech and cloned into a PGL4.23-luciferase vector, and the DNA sequences of all targets are listed in table S5. Transcription factor–expressing plasmids, promoter-luciferase plasmids, and the pRL-TK-*Renilla* constructs as internal controls were cotransfected into 293FT cells on 96-well plates using the X-Transcell reagent (bjyf-Bio technology) following the manufacturer's protocol. Cell extracts were prepared 48 hours after transfection using the lysis buffer provided in the Dual-Luciferase Reporter Assay System Kit (Promega), and luciferase activity was measured on a Synergy Neo2 Multi-Mode Microplate Reader instrument (Bio-Tek) according to the manufacturer's protocol. *Renilla* luciferase activity was used to normalize the firefly luciferase activity.

Statistical analysis

All experiments reported here were independently repeated at least three times, and all values in the figures are depicted as mean ± SEM unless stated otherwise. We used Excel 2016 or GraphPad Prism 7 to perform statistical analyses. No samples or animals were excluded from analyses, sample size estimates were not used, and WT and KO mice in coupled biological replicates were littermates. Investigators were not blinded to mouse or cell genotype during the experiments, and all *P* values are described in the corresponding figure legends or results.

SUPPLEMENTARY MATERIALS

Supplementary material for this article is available at https://science.org/doi/10.1126/sciadv.abn1606

View/request a protocol for this paper from *Bio-protocol*.

REFERENCES AND NOTES

1. M. A. Handel, J. C. Schimenti, Genetics of mammalian meiosis: Regulation, dynamics and impact on fertility. *Nat. Rev. Genet.* **11**, 124–136 (2010).
2. S. Keeney, C. N. Giroux, N. Kleckner, Meiosis-specific DNA double-strand breaks are catalyzed by Spo11, a member of a widely conserved protein family. *Cell* **88**, 375–384 (1997).
3. D. Zickler, N. Kleckner, Recombination, pairing, and synapsis of homologs during meiosis. *Cold Spring Harb. Perspect. Biol.* **7**, (2015).
4. E. D. Parvanov, H. Tian, T. Billings, R. L. Saxl, C. Spruce, R. Aithal, L. Krejci, K. Paigen, P. M. Petkov, PRDM9 interactions with other proteins provide a link between recombination hotspots and the chromosomal axis in meiosis. *Mol. Biol. Cell* **28**, 488–499 (2017).
5. C. Spruce, S. Dlamini, G. Ananda, N. Bronkema, H. Tian, K. Paigen, G. W. Carter, C. L. Baker, HELLS and PRDM9 form a pioneer complex to open chromatin at meiotic recombination hot spots. *Genes Dev.* **34**, 398–412 (2020).
6. S. Wu, Y. C. Hu, H. Liu, Y. Shi, Loss of YY1 impacts the heterochromatic state and meiotic double-strand breaks during mouse spermatogenesis. *Mol. Cell. Biol.* **29**, 6245–6256 (2009).
7. A. H. Peters, D. O'Carroll, H. Scherthan, K. Mechtler, S. Sauer, C. Schofer, K. Weipoltshammer, M. Pagani, M. Lachner, A. Kohlmaier, S. Opravil, M. Doyle, M. Sibilia, T. Jenuwein, Loss of the Suv39h histone methyltransferases impairs mammalian heterochromatin and genome stability. *Cell* **107**, 323–337 (2001).
8. K. Hayashi, K. Yoshida, Y. Matsui, A histone H3 methyltransferase controls epigenetic events required for meiotic prophase. *Nature* **438**, 374–378 (2005).
9. K. Hasegawa, H. S. Sin, S. Maezawa, T. J. Broering, A. V. Kartashov, K. G. Alavattam, Y. Ichijima, F. Zhang, W. C. Bacon, K. D. Greis, P. R. Andreassen, A. Barski, S. H. Namekawa, SCML2 establishes the male germline epigenome through regulation of histone H2A ubiquitination. *Dev. Cell* **32**, 574–588 (2015).
10. S. Maezawa, M. Yukawa, K. G. Alavattam, A. Barski, S. H. Namekawa, Dynamic reorganization of open chromatin underlies diverse transcriptomes during spermatogenesis. *Nucleic Acids Res.* **46**, 593–608 (2018).
11. S. Abhiman, L. M. Iyer, L. Aravind, BEN: A novel domain in chromatin factors and DNA viral proteins. *Bioinformatics* **24**, 458–461 (2008).
12. X. Lin, M. Han, L. Cheng, J. Chen, Z. Zhang, T. Shen, M. Wang, B. Wen, T. Ni, C. Han, Expression dynamics, relationships, and transcriptional regulations of diverse transcripts in mouse spermatogenic cells. *RNA Biol.* **13**, 1011–1024 (2016).
13. S. K. Mahadevaiah, J. M. Turner, F. Baudat, E. P. Rogakou, P. de Boer, J. Blanco-Rodriguez, M. Jasin, S. Keeney, W. M. Bonner, P. S. Burgoyne, Recombinational DNA double-strand breaks in mice precede synapsis. *Nat. Genet.* **27**, 271–276 (2001).
14. H. Xu, M. D. Beasley, W. D. Warren, G. T. van der Horst, M. J. McKay, Absence of mouse REC8 cohesin promotes synapsis of sister chromatids in meiosis. *Dev. Cell* **8**, 949–961 (2005).
15. A. G. Hinch, P. W. Becker, T. Li, D. Moralli, G. Zhang, C. Bycroft, C. Green, S. Keeney, Q. Shi, B. Davies, P. Donnelly, The configuration of RPA, RAD51, and DMC1 binding in meiosis reveals the nature of critical recombination intermediates. *Mol. Cell* **79**, 689–701.e10 (2020).
16. D. Smedley, R. Hamoudi, Y. J. Lu, C. Cooper, J. Shipley, Cloning and mapping of members of the MYM family. *Genomics* **60**, 244–247 (1999).
17. Y. Shi, F. Lan, C. Matson, P. Mulligan, J. R. Whetstine, P. A. Cole, R. A. Casero, Y. Shi, Histone demethylation mediated by the nuclear amine oxidase homolog LSD1. *Cell* **119**, 941–953 (2004).
18. C. B. Gocke, H. Yu, ZNF198 stabilizes the LSD1-CoREST-HDAC1 complex on chromatin through its MYM-type zinc fingers. *PLOS ONE* **3**, e3255 (2008).
19. Y. J. Shi, C. Matson, F. Lan, S. Iwase, T. Baba, Y. Shi, Regulation of LSD1 histone demethylase activity by its associated factors. *Mol. Cell* **19**, 857–864 (2005).
20. A. Pinhasov, S. Mandel, A. Torchinsky, E. Giladi, Z. Pittel, A. M. Goldsweig, S. J. Servoss, D. E. Brenneman, I. Gozes, Activity-dependent neuroprotective protein: A novel gene essential for brain formation. *Brain Res. Dev. Brain Res.* **144**, 83–90 (2003).
21. V. Ostapcuk, F. Mohn, S. H. Carl, A. Basters, D. Hess, V. Iesmantavicius, L. Lampersberger, M. Flemr, A. Pandey, N. H. Thoma, J. Betschinger, M. Buhler, Activity-dependent neuroprotective protein recruits HP1 and CHD4 to control lineage-specifying genes. *Nature* **557**, 739–743 (2018).
22. K. Luck, D. K. Kim, L. Lambourne, K. Spirohn, B. E. Begg, W. Bian, R. Brignall, T. Cafarelli, F. J. Campos-Laborie, B. Charloteaux, D. Choi, A. G. Coté, M. Daley, S. Deimling, A. Desbuleux, A. Dricot, M. Gebbia, M. F. Hardy, N. Kishore, J. J. Knapp, I. A. Kovács, I. Lemmens, M. W. Mee, J. C. Mellor, C. Pollis, C. Pons, A. D. Richardson, S. Schlabach, B. Teeking, A. Yadav, M. Babor, D. Balcha, O. Basha, C. Bowman-Colin, S. F. Chin, S. G. Choi, C. Colabella, G. Coppin, C. D'Amata, D. De Ridder, S. De Rouck, M. Duran-Frigola, H. Ennajdaoui, F. Goebels, L. Goehring, A. Gopal, G. Haddad, E. Hatchi, M. Helmy, Y. Jacob, Y. Kassa, S. Landini, R. Li, N. van Lieshout, A. MacWilliams, D. Markey, J. N. Paulson, S. Rangarajan, J. Rasla, A. Rayhan, T. Rolland, A. San-Miguel, Y. Shen, D. Sheykhkarimli, G. M. Sheynkman, E. Simonovsky, M. Taşan, A. Tejeda, V. Tropepe, J. C. Twizere, Y. Wang, R. J. Weatheritt, J. Weile, Y. Xia, X. Yang, E. Yeger-Lotem, Q. Zhong, P. Aloy, G. D. Bader, J. D. L. Rivas, S. Gaudet, T. Hao, J. Rak, J. Tavernier, D. E. Hill, M. Vidal, F. P. Roth, M. A. Calderwood, A reference map of the human binary protein interactome. *Nature* **580**, 402–408 (2020).
23. M. J. Mallory, R. Strich, Ume1p represses meiotic gene transcription in Saccharomyces cerevisiae through interaction with the histone deacetylase Rpd3p. *J. Biol. Chem.* **278**, 44727–44734 (2003).
24. S. Esaki, M. G. Evich, N. Erlitzki, M. W. Germann, G. M. K. Poon, Multiple DNA-binding modes for the ETS family transcription factor PU.1. *J. Biol. Chem.* **292**, 16044–16054 (2017).
25. A. R. Bellvé, J. C. Cavicchia, C. F. Millette, D. A. O'Brien, Y. M. Bhatnagar, M. Dym, Spermatogenic cells of the prepuberal mouse. Isolation and morphological characterization. *J. Cell Biol.* **74**, 68–85 (1977).
26. I. da Cruz, R. Rodriguez-Casuriaga, F. F. Santinaque, J. Farias, G. Curti, C. A. Capoano, G. A. Folle, R. Benavente, J. R. Sotelo-Silveira, A. Geisinger, Transcriptome analysis of highly purified mouse spermatogenic cell populations: Gene expression signatures switch from meiotic-to postmeiotic-related processes at pachytene stage. *BMC Genomics* **17**, 294 (2016).
27. F. Zhang, Y. Zhang, X. Lv, B. Xu, H. Zhang, J. Yan, H. Li, L. Wu, Evolution of an X-Linked miRNA family predominantly expressed in mammalian male germ cells. *Mol. Biol. Evol.* **36**, 663–678 (2019).
28. R. Kaul-Ghanekar, A. Jalota, L. Pavithra, P. Tucker, S. Chattopadhyay, SMAR1 and Cux/CDP modulate chromatin and act as negative regulators of the TCRbeta enhancer (Ebeta). *Nucleic Acids Res.* **32**, 4862–4875 (2004).
29. S. Rampalli, L. Pavithra, A. Bhatt, T. K. Kundu, S. Chattopadhyay, Tumor suppressor SMAR1 mediates cyclin D1 repression by recruitment of the SIN3/histone deacetylase 1 complex. *Mol. Cell. Biol.* **25**, 8415–8429 (2005).
30. L. Korutla, R. Degnan, P. Wang, S. A. Mackler, NAC1, a cocaine-regulated POZ/BTB protein interacts with CoREST. *J. Neurochem.* **101**, 611–618 (2007).
31. N. Nakayama, G. Sakashita, T. Nagata, N. Kobayashi, H. Yoshida, S. Y. Park, Y. Nariai, H. Kato, E. Obayashi, K. Nakayama, S. Kyo, T. Urano, Nucleus accumbens-associated protein 1 binds DNA directly through the BEN domain in a sequence-specific manner. *Biomedicine* **8**, (2020).
32. K. M. Sathyan, Z. Shen, V. Tripathi, K. V. Prasanth, S. G. Prasanth, A BEN-domain-containing protein associates with heterochromatin and represses transcription. *J. Cell Sci.* **124**, 3149–3163 (2011).
33. N. Saksouk, T. K. Barth, C. Ziegler-Birling, N. Olova, A. Nowak, E. Rey, J. Mateos-Langerak, S. Urbach, W. Reik, M. E. Torres-Padilla, A. Imhof, J. Dejardin, E. Simboeck, Redundant mechanisms to form silent chromatin at pericentromeric regions rely on BEND3 and DNA methylation. *Mol. Cell* **56**, 580–594 (2014).
34. J. Zhang, Y. Zhang, Q. You, C. Huang, T. Zhang, M. Wang, T. Zhang, X. Yang, J. Xiong, Y. Li, C. P. Liu, Z. Zhang, R. M. Xu, B. Zhu, Highly enriched BEND3 prevents the premature activation of bivalent genes during differentiation. *Science* **375**, 1053–1058 (2022).
35. A. Khan, S. G. Prasanth, BEND3 mediates transcriptional repression and heterochromatin organization. *Transcription* **6**, 102–105 (2015).
36. Q. Dai, A. Ren, J. O. Westholm, H. Duan, D. J. Patel, E. C. Lai, Common and distinct DNA-binding and regulatory activities of the BEN-solo transcription factor family. *Genes Dev.* **29**, 48–62 (2015).
37. M. Ueberschar, H. Wang, C. Zhang, S. Kondo, T. Aoki, P. Schedl, E. C. Lai, J. Wen, Q. Dai, BEN-solo factors partition active chromatin to ensure proper gene activation in Drosophila. *Nat. Commun.* **10**, 5700 (2019).
38. Q. Dai, A. Ren, J. O. Westholm, A. A. Serganov, D. J. Patel, E. C. Lai, The BEN domain is a novel sequence-specific DNA-binding domain conserved in neural transcriptional repressors. *Genes Dev.* **27**, 602–614 (2013).
39. C. Xuan, Q. Wang, X. Han, Y. Duan, L. Li, L. Shi, Y. Wang, L. Shan, Z. Yao, Y. Shang, RBB, a novel transcription repressor, represses the transcription of HDM2 oncogene. *Oncogene* **32**, 3711–3721 (2013).
40. D. Sturm, B. A. Orr, U. H. Toprak, V. Hovestadt, D. T. W. Jones, D. Capper, M. Sill, I. Buchhalter, P. A. Northcott, I. Leis, M. Ryzhova, C. Koelsche, E. Pfaff, S. J. Allen, G. Balasubramanian, B. C. Worst, K. W. Pajtler, S. Brabetz, P. D. Johann, F. Sahm, J. Reimand, A. Mackay, D. M. Carvalho, M. Remke, J. J. Phillips, A. Perry, C. Cowdrey, R. Drissi, M. Fouladi, F. Giangaspero, M. Lastowska, W. Grajkowska, W. Scheurlen, T. Pietsch, C. Hagel, J. Gojo, D. Lotsch, W. Berger, I. Slavc, C. Haberler, A. Jouvet, S. Holm, S. Hofer, M. Prinz, C. Keohane, I. Fried, C. Mawrin, D. Scheie, B. C. Mobley, M. J. Schniederjan, M. Santi, A. M. Buccoliero, S. Dahiya, C. M. Kramm, A. O. von Bueren, K. von Hoff, S. Rutkowski, C. Herold-Mende, M. C. Fruhwald, T. Milde, M. Hasselblatt, P. Wesseling, J. Rossler, U. Schuller, M. Ebinger, J. Schittenhelm, S. Frank, R. Grobholz, I. Vajtai, V. Hans, R. Schneppenheim, K. Zitterbart, V. P. Collins, E. Aronica, P. Varlet, S. Puget, C. Dufour, J. Grill, D. Figarella-Branger, M. Wolter, M. U. Schuhmann, T. Shalaby, M. Grotzer, T. van Meter, C. M. Monoranu, J. Felsberg, G. Reifenberger, M. Snuderl, L. A. Forrester, J. Koster, R. Versteeg, R. Volckmann, P. van Sluis, S. Wolf, T. Mikkelsen, A. Gajjar, K. Aldape, A. S. Moore, M. D. Taylor, C. Jones, N. Jabado, M. A. Karajannis, R. Eils,

M. Schlesner, P. Lichter, A. von Deimling, S. M. Pfister, D. W. Ellison, A. Korshunov, M. Kool, New brain tumor entities emerge from molecular classification of CNS-PNETs. *Cell* **164**, 1060–1072 (2016).
41. K. Yamasaki, Y. Nakano, S. Nobusawa, Y. Okuhiro, H. Fukushima, T. Inoue, C. Murakami, J. Hirato, N. Kunihiro, Y. Matsusaka, M. Honda-Kitahara, T. Ozawa, K. Shiraishi, T. Kohno, K. Ichimura, J. Hara, Spinal cord astroblastoma with an EWSR1-BEND2 fusion classified as a high-grade neuroepithelial tumour with MN1 alteration. *Neuropathol. Appl. Neurobiol.* **46**, 190–193 (2020).
42. L. M. Williamson, M. Steel, J. K. Grewal, M. L. Thibodeau, E. Y. Zhao, J. M. Loree, K. C. Yang, S. M. Gorski, A. J. Mungall, K. L. Mungall, R. A. Moore, M. A. Marra, J. Laskin, D. J. Renouf, D. F. Schaeffer, S. J. M. Jones, Genomic characterization of a well-differentiated grade 3 pancreatic neuroendocrine tumor. *Cold Spring Harb. Mol. Case Stud.* **5**, a003814 (2019).
43. D. Bourc'his, T. H. Bestor, Meiotic catastrophe and retrotransposon reactivation in male germ cells lacking Dnmt3L. *Nature* **431**, 96–99 (2004).
44. F. Sun, Y. Fujiwara, L. G. Reinholdt, J. Hu, R. L. Saxl, C. L. Baker, P. M. Petkov, K. Paigen, M. A. Handel, Nuclear localization of PRDM9 and its role in meiotic chromatin modifications and homologous synapsis. *Chromosoma* **124**, 397–415 (2015).
45. K.-I. Ishiguro, The cohesin complex in mammalian meiosis. *Genes Cells* **24**, 6–30 (2018).
46. J. Ahringer, NuRD and SIN3 histone deacetylase complexes in development. *Trends Genetics* **16**, 351–356 (2000).
47. S. E. Polo, A. Kaidi, L. Baskcomb, Y. Galanty, S. P. Jackson, Regulation of DNA-damage responses and cell-cycle progression by the chromatin remodelling factor CHD4. *EMBO J.* **29**, 3130–3139 (2010).
48. R. Aleksandrov, R. Hristova, S. Stoynov, A. Gospodinov, The chromatin response to double-strand DNA breaks and their repair. *Cell* **9**, 1853 (2020).
49. Y. Takada, C. Naruse, Y. Costa, T. Shirakawa, M. Tachibana, J. Sharif, F. Kezuka-Shiotani, D. Kakiuchi, H. Masumoto, Y. Shinkai, K. Ohbo, A. H. Peters, J. M. Turner, M. Asano, H. Koseki, HP1γ links histone methylation marks to meiotic synapsis in mice. *Development* **138**, 4207–4217 (2011).
50. E. Beyret, H. Lin, Pinpointing the expression of piRNAs and function of the PIWI protein subfamily during spermatogenesis in the mouse. *Dev. Biol.* **355**, 215–226 (2011).
51. F. Yang, Y. Lan, R. R. Pandey, D. Homolka, S. L. Berger, R. S. Pillai, M. S. Bartolomei, P. J. Wang, TEX15 associates with MILI and silences transposable elements in male germ cells. *Genes Dev.* **34**, 745–750 (2020).
52. A. Nakamura, M. Shirae-Kurabayashi, K. Hanyu-Nakamura, Repression of early zygotic transcription in the germline. *Curr. Opin. Cell Biol.* **22**, 709–714 (2010).
53. A. Suzuki, Y. Saga, Nanos2 suppresses meiosis and promotes male germ cell differentiation. *Genes Dev.* **22**, 430–435 (2008).
54. C. K. Matson, M. W. Murphy, M. D. Griswold, S. Yoshida, V. J. Bardwell, D. Zarkower, The mammalian doublesex homolog DMRT1 is a transcriptional gatekeeper that controls the mitosis versus meiosis decision in male germ cells. *Dev. Cell* **19**, 612–624 (2010).
55. W. Mu, J. Starmer, A. M. Fedoriw, D. Yee, T. Magnuson, Repression of the soma-specific transcriptome by Polycomb-repressive complex 2 promotes male germ cell development. *Genes Dev.* **28**, 2056–2069 (2014).
56. H. Yang, H. Wang, R. Jaenisch, Generating genetically modified mice using CRISPR/Cas-mediated genome engineering. *Nat. Protoc.* **9**, 1956–1968 (2014).
57. E. A. Ahmed, D. G. de Rooij, Staging of mouse seminiferous tubule cross-sections. *Methods Mol. Biol.* **558**, 263–277 (2009).
58. V. Gaysinskaya, I. Y. Soh, G. W. van der Heijden, A. Bortvin, Optimized flow cytometry isolation of murine spermatocytes. *Cytometry A* **85**, 556–565 (2014).
59. M. P. Meers, T. D. Bryson, J. G. Henikoff, S. Henikoff, Improved CUT&RUN chromatin profiling tools. *eLife* **8**, e46314 (2019).
60. H. M. Amemiya, A. Kundaje, A. P. Boyle, The ENCODE Blacklist: Identification of problematic regions of the genome. *Sci. Rep.* **9**, 9354 (2019).

Acknowledgments: We wish to sincerely thank W. Xie (Tsinghua University) for guidance in the use of CUT&RUN; J. Wang and X. Ding of the Institute of Biophysics of the Chinese Academy of Sciences for technical assistance; and S. Li, X. Zhu, X. Yang, and Q. Meng of the Institute of Zoology, Chinese Academy of Sciences, for technical assistance. We thank ACCDON LLC/LetPub (www.letpub.com) for its linguistic assistance during the preparation of this manuscript. **Funding:** This work was supported by the Ministry of Science and Technology of China (2018YFE0201100 and 2016YFC1000606 to C.H.) and the National Natural Science Foundation of China (31771631 and 31970795 to C.H.). **Author contributions:** Conceptualization was performed by C.H., S.D., L.M., and D.X.; methodology and investigation by L.M., D.X., C.H., M.L., S.D., X.L., H.N., C.G. and J.C.; visualization by X.L., L.M., D.X., C.H., and C.G.; supervision by S.D. and C.H.; writing—original draft by L.M., D.X., and C.H.; and writing—review and editing by C.H. **Competing interests:** The authors declare that they have no competing interests. **Data and materials availability:** All data needed to evaluate the conclusions in the paper are present in the paper and/or the Supplementary Materials. All data have been deposited to GEO with the accession number GSE189599.

Submitted 8 November 2021
Accepted 8 April 2022
Published 25 May 2022
10.1126/sciadv.abn1606